Model Validation and Performance Analyses for MEMS Design

by

Ozan Anaç

A Thesis Submitted to the

Graduate School of Engineering

in Partial Fulfillment of the Requirements for

the Degree of

Master of Science

in

Mechanical Engineering

Koç University

September 2006

Koç University

Graduate School of Sciences and Engineering

This is to certify that I have examined this copy of a master's thesis by

Ozan Anaç

and have found that it is complete and satisfactory in all respects,

and that any and all revisions required by the final

examining committee have been made.

Committee Members:

İpek Başdoğan, Ph. D. (Advisor)

Alphan Sennaroğlu, Ph. D.

Çağatay Başdoğan, Ph. D.

Date: 12 September 2006

ABSTRACT

Micro Electro Mechanical Systems (MEMS) are among the new and emerging technologies of the future and have many applications in different disciplines. Predicting the performance of such systems early in the design process can significantly impact the design cost and also improve the quality of the design. This thesis presents the model validation and design methodologies developed to predict the performance of the micro systems. A two-dimensional micro scanner mirror was chosen as the case study to demonstrate the developed methodologies. The model validation methodology includes the verification of the finite element model using an experimental modal analysis setup for measuring the out-of-plane vibrations of the micro devices. The setup includes a laser doppler vibrometer (LDV) that is used to pick up signals without contacting the micro structure. An experimental procedure was developed to collect the vibration data and then the data were processed by using MATLAB and modal analysis software ME'scope. The finite element analysis and experimental results were compared to identify the inaccuracies in the modeling assumptions. Validated finite element model was used to obtain the state space representation of the microscanner mirror to proceed further with additional design studies. The state space model was used for disturbance analysis which was performed using Lyapunov approach to obtain root mean square (RMS) values of the mirror rotation angle under the effect of a disturbance torque. The disturbance analysis framework was combined with the sensitivity analysis to determine the critical design parameters for improving the system performance. In addition to the disturbance sensitivity analysis, modal sensitivities of the design parameters were also investigated. This analysis was conducted by perturbing the design parameters and investigating the change in the modal frequencies.

Another study that was conducted in this thesis was the prediction of the modal frequencies of the micro device using analytical formulations. Although this analysis is very specific to the micro device used in this thesis, it may provide valuable information to the engineer at the initial design stage especially when high frequency requirements and separation of vibration modes are very critical.

The in-plane vibration setup and the measurement procedure is also explained in this thesis for completeness. However, the results of the in-plane measurements are not available currently and left for a future work.

ÖZET

Mikro-elektro-mekanik sistemler geleceğin yeni ve gelişen teknolojileri arasında yer almaktadır ve çok çeşitli alanlarda uygulamaları bulunmaktadır. Bu tarz sistemlerin performanslarını tasarım sürecinde önceden tahmin etmek, tasarım maliyetini büyük ölçüde düşürürken, tasarım kalitesini de arttırabilir. Bu çalışmada, mikro sistemlerin performanslarını önceden saptamak için geliştirilen model doğrulama ve tasarım metotları sunulmaktadır. Geliştirilen metotları uygulamak için iki boyutlu bir mikro tarayıcı ayna örnek sistem olarak seçilmiştir. Model doğrulama metodu, sonlu elemanlar yöntemiyle oluşturulmuş modelin, mikro sistemlerin düzleme dik olan titreşimlerini ölçmek için kullanılan deneysel modal analiz düzeneği yardımıyla doğrulanmasını içermektedir. Deney düzeneğinde titreşim sinyallerini mikro sisteme temas etmeden ölçmek için Laser Doppler Vibrometer (LDV) kullanılmaktadır. Mikro sistemdeki titreşim sinyallerini ölçmek için deneysel bir yöntem geliştirilmiş ve bu yöntemle toplanan veriler MATLAB ve bir modal analiz programı olan ME'scope kullanılarak işlenmiştir. Sonlu elemanlar modeli ve deneysel sonuçlar, modeldeki kusurları ortaya çıkarmak için karşılaştırılmıştır. Doğrulanan sonlu elemanlar modeli, yeni tasarım çalışmaları için oluşturulan durum-yer (state-space) gösterimini elde etmek için kullanılmıştır. Tarayıcı aynanın bozunma analizlerinde (Disturbance Analysis), bozucu tork etkisi altındaki aynanın dönme açısının standart sapması (RMS) Lyapunov yaklaşımı yardımıyla hesaplanmış ve bu işlem için de durum-yer modeli kullanılmıştır. Sistem performansını arttırmak üzere kullanılacak kritik tasarım parametrelerini saptamak için, bozunum analizleri, bozunum hassasiyet analizleri (Disturbance Sensitivity Analysis) ile birleştirilmiştir. Bozunum hassasiyet analizlerine ek olarak tasarım parametrelerinin modal hassasiyetleri de incelenmiştir. Bu analiz, tasarım parametrelerinde küçük değişiklikler yaparak sistemin doğal frekanslarının buna bağlı değişimlerinin gözlenmesiyle oluşturulmuştur.

Bu tezde sunulan bir başka çalışma da, analitik formüller yardımıyla mikro sistemin doğal frekanslarının hesaplanmasıdır. Bu çalışma, bu tezde kullanılan mikro sisteme özgü olmasına rağmen, tasarımda yüksek frekans koşulları ve sistemin belli doğal frekanslarının birbirinden ayrılması söz konusu ise erken tasarım aşamasında tasarımcı mühendis için çok değerli bir bilgi olabilir.

Düzlem içindeki titreşimlerin ölçülmesinde kullanılabilecek bir deney düzeneği ve ölçüm metodu da bu tezde bütünlüğü sağlamak için sunulmuştur. Fakat, düzlem içi titreşim ölçümlerinin sonuçları şu anda mevcut değildir ve gelecekte yapılacak çalışmalara bırakılmıştır.

ACKNOWLEDGEMENTS

I would like to express my sincere gratitude to my thesis advisor Dr. İpek Başdoğan for giving me the opportunity to carry out this thesis work within her research team. I appreciate Koç University College of Engineering for supporting me through travel grants that enabled me to participate international conferences. Moreover, I would like to thank the Scientific and Technological Research Council of Turkey (TUBITAK) for the scholarship which enabled me to cover my living expenses.

I also would like to thank Dr. Alphan Sennaroğlu and Dr. Çağatay Başdoğan for taking part in my thesis jury. I would also like to thank Dr. Hakan Ürey for giving me the opportunity to work in his laboratory and for his valuable guidance.

As my colleagues, many thanks to Ihsan Günev for his support during building up my experimental setup and procedure and his friendship during the lab hours. The OML staff Çağlar Ataman, Olgaç Ergeneman and Arda Yalçınkaya for their hospitability and information on experimental knowledge. To Emre Dikmen for his support on theoretical background and friendship on the international and national conferences. Of course, my appreciations and gratitude go to İbrahim Büküşoğlu and Murat Danışman for their incredible friendship from day and night as a roommate.

Finally, I would like to thank the ANAÇ family including İlyas Bey, Necla Hanım, Emir and Tuğçe Ece. Even though you were not here with me, none of these would have been possible without you.

TABLE OF CONTENTS

List of Tables x

List of Figures xi

Chapter 1: Introduction 1

1.1 Generalized Design Approach………………………………………………... 1

1.2 2D MEMS Mirror for Case Study............……………...…………………….. 4

1.3 Main Contributions and Thesis Outline……….……………………………8

Chapter 2: Vibrational Analysis of the 2D Scanner 10

2.1 Introduction……………………………………………………………………10

2.2 Experimental Analysis………………………………………………………...10

2.2.1 Experimental Setup for Out-of-plane Measurements..................... 11

2.2.1.1 Laser Doppler Vibrometer (LDV)………………………...13

2.2.1.2 Microscope System………………………………………14

2.2.1.3 Camera and Laser Positioning………............................... 14

2.2.1.4 Software and Data Acquisition…………………………... 15

2.2.2 Experimental Procedure for Out-of-Plane Measurements…………15

2.2.3 Experimental Setup for In-Plane Measurements…………………... 23

2.2.3.1 Principle of Operation…………………………………....23

2.2.3.2 In-Plane Motion Analysis Setup…………………………... 24

2.2.4 Results of the Experimental Analysis……………………………….27

2.3 Finite Element Analysis……………………………………………………28

2.3.1 Results of Finite Element Analysis…………………………………...32
2.4 Analytical Formulations……………………………………………………34
2.4.1 Results of Theoretical Analysis……………………………………….39

Chapter 3: Validation of the FEM and State Space Representation of the 2D Scanner **40**
3.1 Introduction……………………………………………………………....40
3.2 Comparison of Experimental, Numerical and Analytical Results……….… 40
3.3 State Space Modeling……………………………………………………….44
3.4 State Space Model Generation of 2D Micro Scanner Mirror…………….....49

Chapter 4: Design Analysis **52**
4.1 Introduction……………………………………………………………....52
4.2 Disturbance Analysis…………………………………………………..... 52
4.3 Disturbance Sensitivity Analyses…………………………………………….. 58
4.4 Modal Sensitivity Analysis………………………………………………… 61

Chapter 5: Discussion and Conclusion **64**

Bibliography **67**

Publications **71**

Vita **72**

LIST OF TABLES

Table - 2.1 Experimental modal analysis results..28

Table - 2.2 Results of the finite element modal analysis..33

Table - 2.3 Parameters used for calculating the theoretical modal frequencies of the 1-D micro scanner [34].. 36

Table - 2.4 Mass and Mass moment of inertia for different mirror shapes [34].. 36

Table - 2.5 Theoretical frequency results for Bimag micro scanner mirror............ 39

Table - 3.1 Comparison chart for modal analysis results..41

Table - 3.2 Table for error values calculated according to Equation (3.1)............. 42

Table - 4.1 RMS values for torque disturbances..58

Table - 4.2 Disturbance Sensitivity Analysis..60

Table - 4.3 Table for modal sensitivity calculations for different physical parameters..62

LIST OF FIGURES

Figure-1.1 Flow chart for the developed generalized design approach.................. 3
Figure-1.2 (a) Retinal Scanning Display Technology of Microvision, Inc uses a 2D MEMS microscanner. (Photo courtesy of Microvision, Inc). (b) Hand-held barcode readers are potential applications of MEMS microscanners... 5
Figure-1.3 Conceptual optics of the retinal scanning beam display (RSD). The final image on the retina is a two-dimensional raster pattern [12]..6
Figure-1.4 (a) Schematic of the biaxial microscanner (b) Bi-axial MEMS scanner die photo[12]...7
Figure-2.1 Picture of the overall setup..12
Figure-2.2 Schematic of the experimental setup for out-of-plane measurements....12
Figure-2.3 OFV-551 Fiber Interferometer...13
Figure-2.4 Experimental procedure to collect, process and visualize the measured data 16
Figure-2.5 (a) Picture of the mirror with grids and measurement points. (b) The photo while matching the real image and transparent (ghost) image of the mirror...17
Figure-2.6 LabView program screen shot..18
Figure-2.7 An example that relates the excitation input to velocity output at points a) 11 and b) 3 (referred to Figure-2.5-a) 19
Figure-2.8 Screenshot of ME'scope for the transferred data between 360-420 Hz range..19

Figure-2.9 Screenshot of ME'scope while generating the experimental model.......20
Figure-2.10 Shape table derived in ME'scope for complete experimental modal analysis of the MEMS micro mirror..21
Figure-2.11 Stroboscopic illumination phenomenon...24
Figure-2.12 Setup for in-plane analysis...25
Figure-2.13 Inside view of stroboscopic illumination device................................ 26
Figure-2.14 Finite element model of 2D micro mirror using 3D elements............. 30
Figure-2.15 One dimensional torsional resonant scan mirror suspended with two flexure beams that are fixed at the ends. The inset shows the critical dimensions and coordinate axis that are used for driving the formulae at Table-2.3 [34]...35
Figure-2.16 One mass one spring system... 35
Figure-2.17 Schematic of the outer frame and the mirror [12]...............................38
Figure-2.18 Two mass and two spring system... 38
Figure-3.1 Numbered Schematic of Bimag Scanner mirror.................................43
Figure-3.2 Mass-Spring-Damper system...44
Figure-3.3 Example transfer functions for 2D microscanner
a) Torque applied at point 2 and rotational displacement measured at point 3.
b) Torque applied at point 3 and rotational displacement measured at point 1.. 51
Figure-4.1 The frequency response and phase diagrams for the disturbance filter. The magnitude falls down quickly after the corner frequency........... 55
Figure-4.2 Disturbance shaping filter in series with plant model.........................56

Chapter 1

INTRODUCTION

Predicting the performance of micro systems accurately early in the design process can reduce the cost of prototyping and also improve the effectiveness and reliability of the micro device. In this thesis, a design approach which includes modeling and testing techniques for predicting the performance of the micro systems is presented. A two dimensional torsional microscanner mirror is chosen as the case study to demonstrate the developed methodologies. This chapter describes the details of the microscanner mirror and summarizes the generalized design approach that was developed in this study. Main contributions of this thesis and the thesis outline are also included in this chapter.

1.1 Generalized Design Approach

Dynamic performance and reliability of micro devices are important factors that have to be considered early in the design process for improving the effectiveness of the final product. Many design approaches have been developed in order to improve the quality of the micro devices. The approach that was developed by [1] uses the genetic algorithms for mask layout design and improves the quality of the fabrication early in the design phase. Another approach uses the genetic algorithms in order to create an automated design synthesis [2]. Also, structured design synthesis by using a nodal simulation approach and synthesis of different energy domains were introduced in another study [3]. Moreover, a hierarchical design approach [4] was introduced for optimization and design automation of MEMS.

Our design methodology aims at predicting the end-to-end system performance of the micro systems using experimental and numerical techniques. If the performance of the system does not meet the requirements, the design tools developed in this thesis can be used to identify the critical design parameters. Then, these parameters may be the focus of the redesign efforts that attempt to improve the performance. Figure-1.1 summarizes the design approach introduced in this thesis.

The first step in our design approach is the parallel process of building the experimental setup and Finite Element Model (FEM) for dynamic characterization of the micro device. Step 2 involves performing experimental and numerical modal analysis. The details of the experimental setup and finite element model will be explained in Sections 2.2 and 2.3, respectively. The validity of the finite element model is critical in determining the confidence level required for performing further design analysis. The model predictions are compared with the experimental measurements to identify the inaccuracies in the modeling assumptions. The next step (step 4) involves updating and correcting the model and also improving the experimental measurement techniques to have a better match between the measured and predicted results. If the FEM predicts the mode shapes and modal frequencies accurately, the FEM is considered to be validated and it can be used for further design analysis (step 5). Step 5 includes various types of design studies to improve or to proceed with the current design. The first design study conducted in this thesis requires building the state space representation of the micro device. Once the state space representation of the system is built, the system performance under the anticipated disturbance conditions can be predicted using the disturbance analysis framework which is outlined in Chapter 4. The disturbance analysis is conducted using Lyapunov approach. The disturbance analysis results tell us whether the system is able to meet the design requirements or not. If the requirements are met, we may consider proceeding with the current design. If the requirements are not met, then the designer can perform a sensitivity analysis to identify the critical design parameters for improving the system performance under the effect of the disturbance sources. Sensitivity information provides the performance change of a system with respect to changing design parameters [5-7].

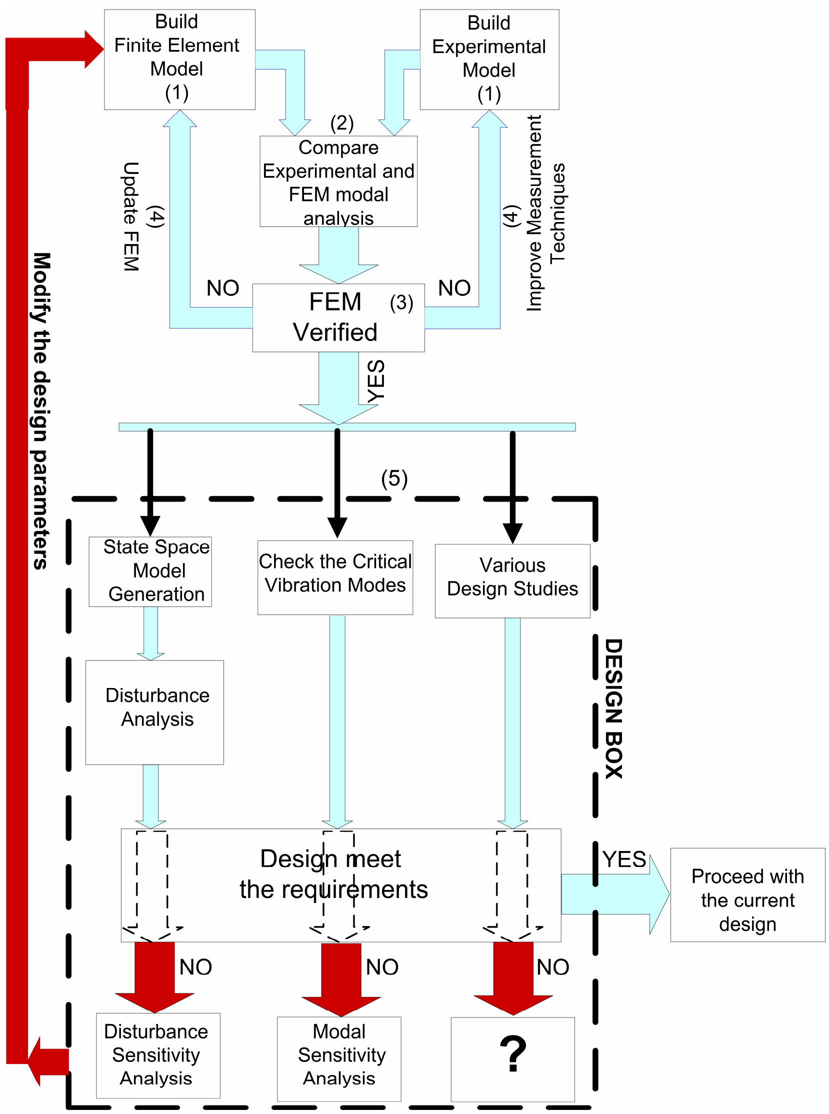

Figure-1.1 Flow chart for the developed generalized design approach

The second design study studies the effect of the design parameters on the critical vibration modes. For that purpose, the critical modes are determined and if high frequency requirements and/or separation of critical vibration modes are not achieved, modal sensitivity of the design parameters can be performed and critical design parameters can be identified. There is also another box in Step 5 which is called “various design studies” which refers to the possible studies that can be done using the validated FEM. For example: transient analysis and/or harmonic analysis can be performed with the validated FEM considering the design constraints and requirements of the specific application. After these design studies are completed, the required changes can be made and this process can continue until the requirements are met.

1.2 2D MEMS Mirror for Case Study

A microscanner is a tiny movable mirror that can scan or steer a laser beam in 1D, 2D or 3D. Due to their promising mechanical, optical and electrical properties, there has been a significant amount of research and development efforts on microscanners and micromirror technologies [8]. The fundamental application field of MEMS microscanners is the display and imaging systems. Fast scanning speeds and high scan angles achieved by the microscanner technologies make them a good candidate for this type of applications [9]. Today, micromirrors and micro scanners offer effective solutions for problems from different engineering professions. Some of the major application areas of micromirror and microscanner technologies are ‘Retinal Scanning Display’ [10] and ‘Barcode Readers’ [11] (See Figure-1.2).

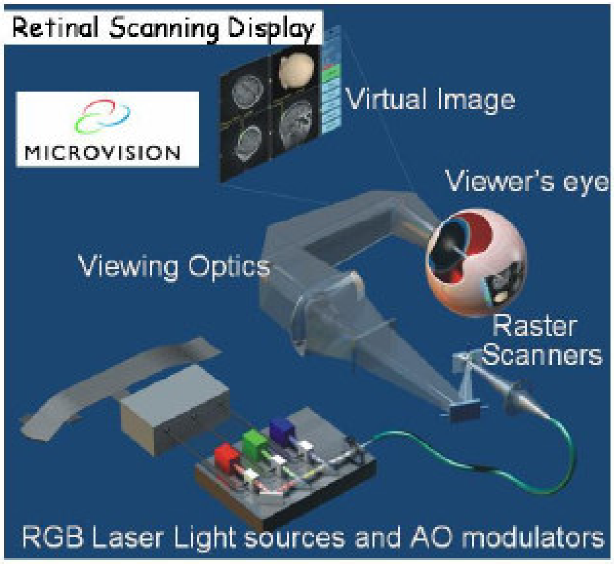

(a) (b)

Figure-1.2 (a) Retinal Scanning Display Technology of Microvision, Inc uses a 2D MEMS microscanner. (Photo courtesy of Microvision, Inc)
(b) Hand-held barcode readers are potential applications of MEMS microscanners

A two-dimensional torsional micro scanner mirror is chosen as the case study to demonstrate the developed methodologies. The mirror is being used in 'Retinal Scanning Display' (RSD) which is a head mounted micro-display developed by Microvision, Inc. RSD utilizes a single two dimensional MEMS microscanner for scanning video data onto the retina of the user [10]. The mirror producing angular motion is used to deflect a modulated light beam on an image plane to create a display (see Figure-1.3). In order to construct a two-dimensional rasterlike rectangular image, the biaxial mirror is rotated about two orthogonal axes at different frequencies. The beam from the light source is sent to the MEMS scanner and focused onto an intermediate image plane with collection optics. The position of this focus point is determined by the angle of the scanning mirror. During the operation, the mirror is scanned bi-axially, creating a 2-dimensional pattern onto the intermediate image plane. A set of relay optics is used to relay this image pattern onto the viewer's eye. The focused spot position on the retina is a direct function of the bi-axial angles of the mirror [12].

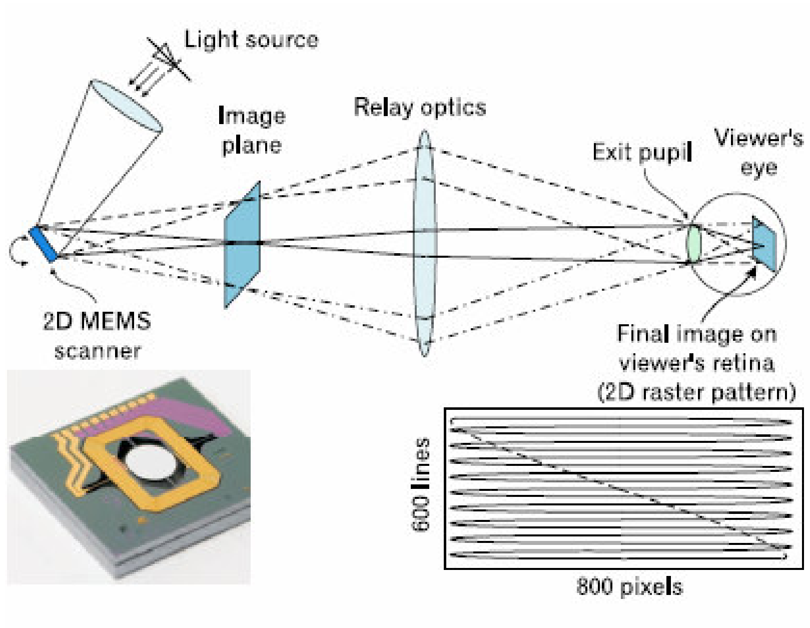

Figure-1.3 Conceptual optics of the retinal scanning beam display (RSD). The final image on the retina is a two-dimensional raster pattern [12].

The outer frame of the device is actuated in two axes using an electromagnetic torque, created by a single coil interacting with an external magnet placed at 45° to the orthogonal axis (See Figure-1.4). This novel actuation technique allows producing large scan angles at low actuation powers due to high mechanical quality factors obtained in air. Since there is no direct electrical or mechanical loading on the scan mirror, exceptionally high quality factors are obtained in air [12].

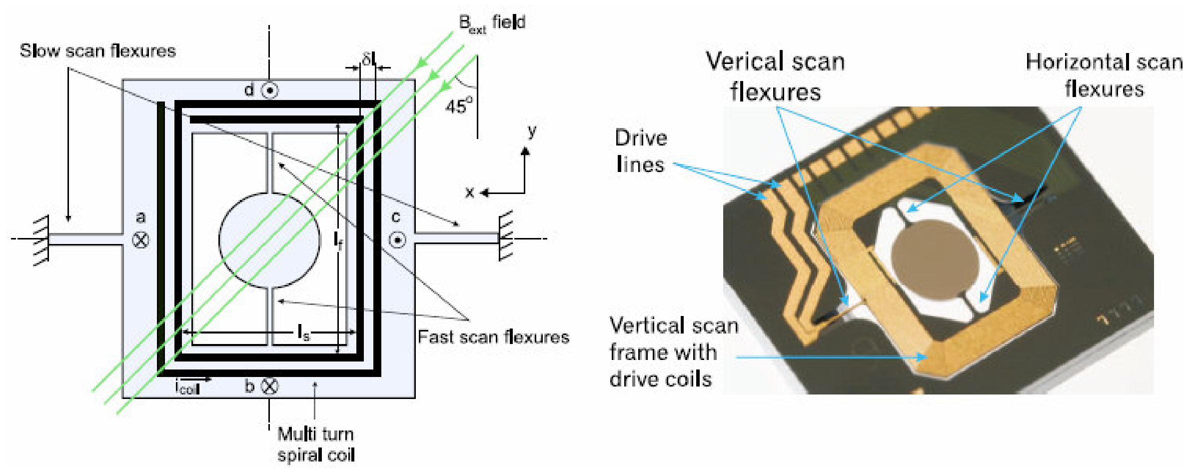

(a) (b)

Figure-1.4 (a) Schematic of the biaxial microscanner (b) Bi-axial MEMS scanner die photo [12].

Dynamic display and imaging applications demand high performance scanners, which have high frequency (exceeding 10 kHz), large scan-angle–mirror size product (>±10deg.mm), good optical surface quality (<λ/20 static and dynamic flatness), high sensitivity position sensors, and high-torque actuators that are compact and low power [13]. Furthermore, one of the most important system design goals is to obtain good separation of vibration modes with respect to torsion [13]. In order to achieve high frequency requirements and separation of critical vibration modes; modal characteristics of the mirrors should be investigated and understood carefully for improving the quality of the design. The scanning capability of such micro scanners can be significantly impacted by the disturbances coming from the outside sources. Since these devices are electro-statically or electro-magnetically actuated, driving electronics jitter, control loop sensor errors and thermal changes in the environment are the examples of disturbances that may affect the performance of the mirror during the operation mode.

1.3 Main Contributions and Thesis Outline

The thesis focuses on developing a methodology in order to predict and improve the performance of micro systems early in design phase using an experimentally validated finite element model.

Main contributions of the thesis can be summarized as follows:

- An experimental modal analysis setup was built and a procedure for measuring the dynamic performance of micro systems was developed.
- A methodology was developed to validate the FEM using the experimentally measured data.
- The performance of the micro device was predicted under the anticipated disturbance sources.
- The critical parameters that affect the performance of the system under the anticipated disturbance sources were identified.
- Modal sensitivity analysis was performed to identify the design parameters that affect the critical vibration modes.
- A generalized design methodology for predicting and improving the performance of micro devices was presented.

Thesis outline can be summarized as follows:

Chapter 2 describes our efforts in determining the dynamic characteristics of the 2D microscanner. Details of the experimental, numerical and analytical vibration analysis of the 2D scanner mirror are included in Chapter 2.

The comparison of the experimental, numerical and analytical results is given in Chapter 3. Moreover, this chapter includes the detailed information for generation of the state space model which uses the eigenvalues and eigenvectors that are extracted from the ANSYS modal analysis results.

Chapter 4 summarizes the design studies conducted on the 2D micro mirror. The design studies include disturbance analysis, disturbance sensitivity analysis and modal sensitivity analysis. The disturbance analysis investigates the variation of mirror rotation under the effect of disturbance sources. The disturbance sensitivity analysis identifies critical design parameters for improving the performance of the micro system under the anticipated disturbance sources. Last study conducted in Chapter 4 is the modal sensitivity analysis which is defined as the change of the modal frequency of a system according to a physical parameter change. In this study, the critical design parameters for specific vibration modes are identified.

Chapter 2

VIBRATIONAL ANALYSIS OF THE 2D SCANNER

2.1 Introduction

This section summarizes our efforts in determining the dynamic characterization of the 2D microscanner. In order to determine the mode shapes and the modal frequencies of the micro device, we built an experimental modal analysis setup. Section 2.2 describes the details of the setup and the procedure to make the measurements. Section 2.3 describes the details of the FEM to perform the numerical modal analysis of the micro device. Section 2.4 summarizes the analytical formulations used to calculate the modal frequencies of the 2D scanner to support the design efforts.

2.2 Experimental Analysis

Experimental modal analysis techniques are traditionally used for dynamic characterization of “macro” systems and it is a very well established area. However, for micro systems modal testing is a fairly new field and advanced testing equipment and methods are required for the dynamic characterization of MEMS. Overviews of the measuring techniques for micro structures are given in [14] and [15]. Most of these systems measure out-of-plane and in-plane vibrations by means of stroboscopic interferometry [16-18]. Another system that uses the commercial Polytec Laser Doppler Vibrometer for measuring out-of-plane vibrations is described in [15]. Furthermore, there are studies which have used the single point Polytec vibrometer for modal analysis by scanning the entire surface point by point to determine deflection shapes and natural frequencies of the structure [19-21].

A modal analysis testing system was built for micro systems in our laboratory. The setup includes a laser doppler vibrometer (LDV) that is used to pick up signals without contacting the micro structure in order to measure the out-of-plane vibrations of micro systems. The LDV sensor head utilizes flexible fiber-optics and an output lens to deliver the laser probe to the measurement point and to collect the reflected light as an input to the interferometer. The micro mirror is excited at a wide frequency range and the velocity data measured by LDV is collected through the use of a data acquisition card and a LabView program that is developed in our laboratory. The frequency response functions (FRF) that relate the excitation input to velocity output are measured at various locations of the micro structure and then transferred to modal analysis software, ME'scope, to extract the modal parameters. The experimental setup details and the procedure for out-of-plane dynamic measurements of micro devices can be found at Section 2.2.1 and 2.2.2, respectively. In order to have complete information about the dynamic behavior of the system in 3D, in-plane vibration measurements are also required. In-plane measurements can be done using a different technique which is called "stroboscopic illumination". The setup and the procedure are being currently developed in our laboratory for in-plane vibration measurements. Details will be given in Section 2.2.3.

2.2.1 Experimental Setup for Out-of-plane Measurements

This section summarizes the technical specifications of the equipment that we use to build the modal testing system for out-of-plane measurements (See Figure-2.1 and 2.2).

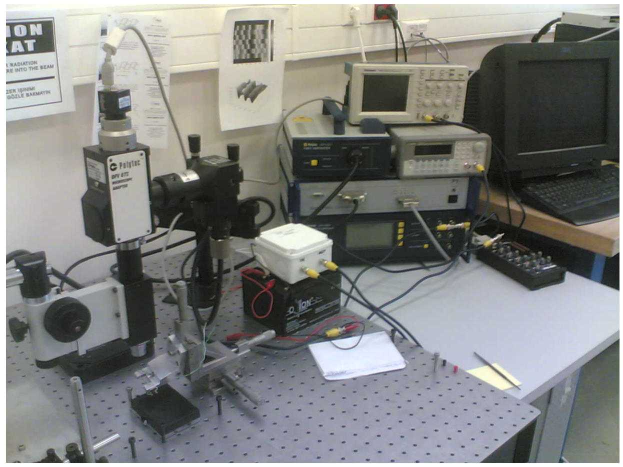

Figure-2.1 Picture of the overall setup

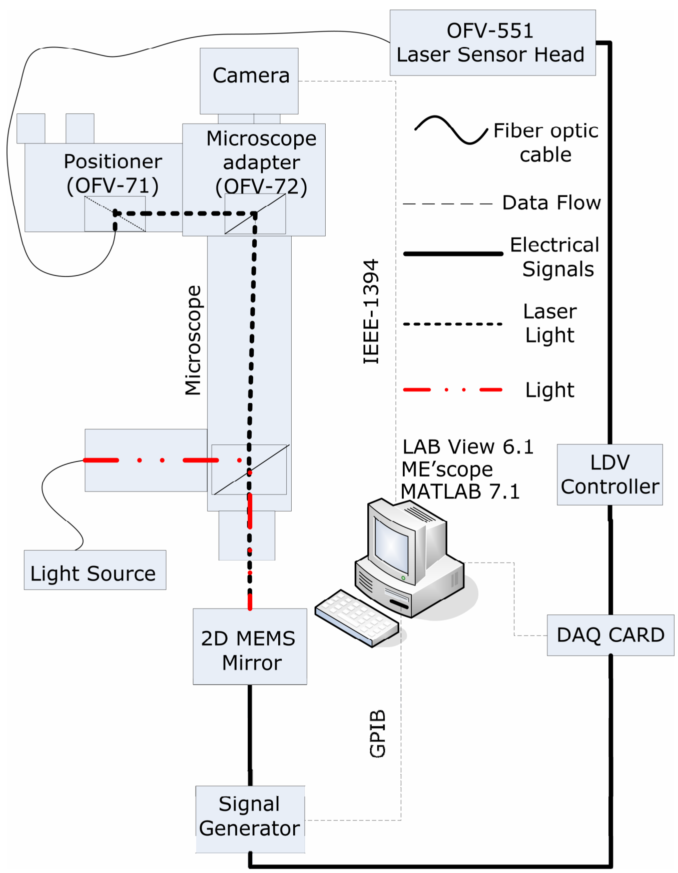

Figure-2.2 Schematic of the experimental setup for out-of-plane measurements

2.2.1.1 Laser Doppler Vibrometer (LDV)

Polytec Fiber Optic Vibrometer is used for vibration measurements [22]. Polytec Laser Doppler Vibrometers operate on the Doppler principle, measuring back-scattered laser light from a vibrating structure, to determine its vibrational velocity and displacement only in out-of-plane direction. The fiber-optic vibrometer is composed of the OFV-5000, vibrometer controller and an OFV-551 fiber interferometer (Figure-2.3). The OFV-551 sensor head utilizes flexible fiber-optic cable together with a focusing lens to deliver the laser light to the measurement point and to collect the reflected light as an input to the interferometer [22]. OFV-551 is an optical laser head which is a 633 nm wavelength He-Ne laser source with red laser beam. It has a spot size of 2.1 µm through the use of the microscope. The controller, OFV-5000, provides signals and power for the sensor head, and processes the vibration signals. The vibration signals are electronically converted by decoders within the controller to obtain velocity and displacement information. The controller uses the wide bandwidth velocity decoder, VD-02. The decoder has four ranges (5 mm/s/V, 25 mm/s/V, 125 mm/s/V, 1000 mm/s/V) with resolution 0.15 µm/s and it can detect signals up to 10 m/s. It has an upper frequency limit of 1.5 MHz.

Figure-2.3 OFV-551 Fiber Interferometer

2.2.1.2 Microscope System

Microscope system consists of three main parts that are VM-1V Video adaptable microscope, Meiji – S. Plan M5X objective, and Meiji FL150 light source with halogen lamp. VM-1V microscope can be adapted to a CCD camera and can be used with all kind of infinity corrected lenses. A field of view of 0.96 mm X 0.72 mm can be achieved with the VM-1V microscope using 1/3" CCD camera with 5X magnification objective. Meiji- S Plan M5X objective is an infinity corrected objective with 0.10 numerical aperture and depth of focus of 55 µm. Meiji FL-150 light source is 150 W halogen lamp which is used with flexible single arm light guide for adapting the light source to the microscope for in-line illumination of the micro device.

2.2.1.3 Camera and Laser Positioning

A CCD camera and a Polytec microscope scan unit (MSV-50) is used for exact positioning of the laser beam for velocity measurements. The CCD camera is a Point Grey-FLEA CCD 1/3" IEEE-1394 camera with 1024x768 resolution with a pixel size of 4.65µmX4.65µm. Polytec microscope scan unit is composed of two main parts which are OFV-71 and OFV-72. OFV-72 is the microscope adapter for the camera and OFV-71 is the manual positioner for the laser beam. The microscope adapter can be equipped with the digital camera, Point Grey-FLEA, to visualize the measurement object and it contains a filter to reduce the viewed intensity of the laser spot when observing mirror-like surfaces [23]. OFV-71 is the manual positioner of the laser beam which contains movable mirrors to deflect the laser beam. It is mainly used for manually positioning of the laser beam to a desired position on the micro device.

2.2.1.4 Software and Data Acquisition

The software programs that are used in this setup are LAB View 6.1, Matlab 7.1 and ME'scope [24-26]. The Lab View is used for interfacing with data acquisition (DAQ) card which is a NI 6034E. The DAQ card has the capability of converting an analog signal to a digital one and the Lab View has the capability of gathering this digital information. In Lab View environment, we can also drive our signal generator, which is an Agilent 33220A 20 MHZ function generator, via GPIB interface. The Matlab image processing and image acquisition toolboxes are used for gathering images of the micro device in order to visualize and locate the laser beam to a specified location. The ME'scope software is used to extract the modal parameters such as modal frequencies, modal damping coefficients and mode shapes from the experimentally measured frequency response functions.

2.2.2 Experimental Procedure for Out-of-Plane Measurements

This section summarizes the experimental procedure (see Figure-2.4) for dynamic testing of micro systems. The experimental modal testing system described in the previous section is utilized to gather, process and visualize the vibration data.

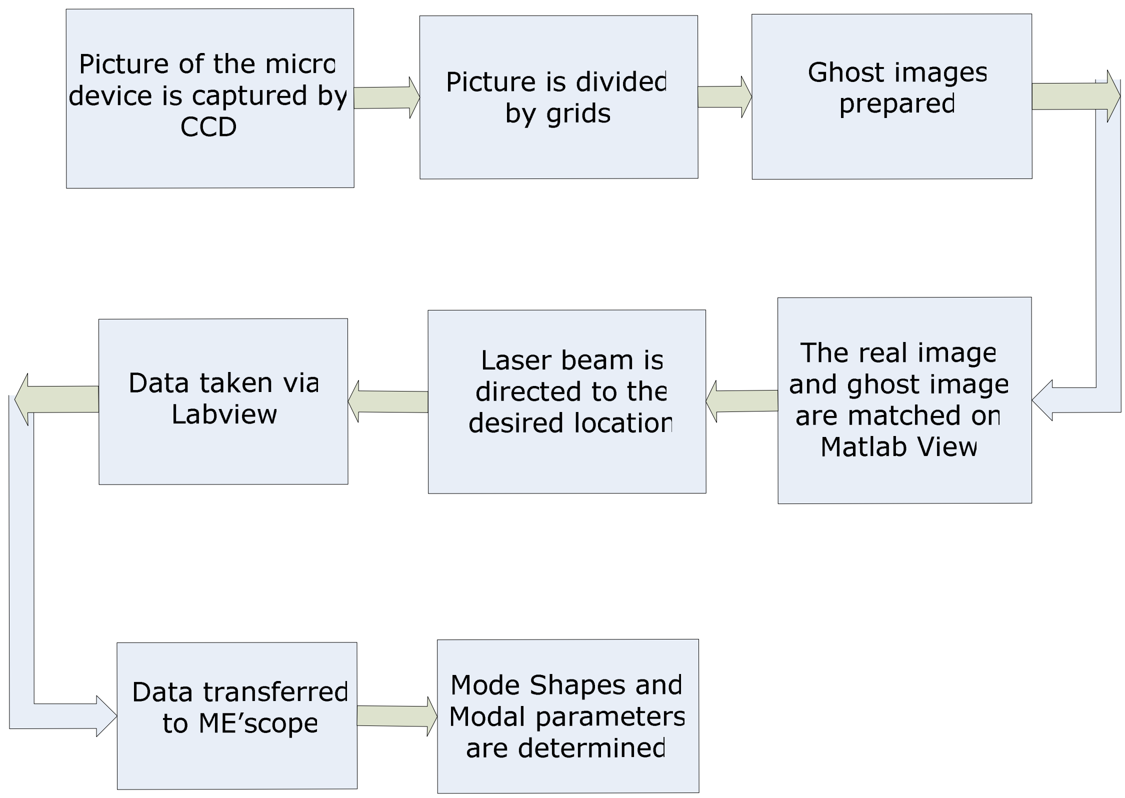

Figure-2.4 Experimental procedure to collect, process and visualize the measured data

At the first step of the experimental procedure, the picture of the micro device is captured by the CCD camera. The picture of the mirror is then divided into grids for determining the measurement points (see Figure-2.5-a). The 'grid' procedure allows the accurate positioning of the laser on the micro device. As we increase the number of measurement points, better results are obtained from the modal analysis software ME'scope.

The next step in the experimental procedure is to divide the image into grids and make it transparent in order to see real video images of the device underneath (Figure-2.5-b). The transparent picture which is called ghost image of the mirror is used as a mask in order to locate the measurement points on the real device. Ghost image is kept frozen using the

Matlab image acquisition toolbox while real time video images are captured. The real time image of the device is matched with the ghost image by the help of an x-y stage on which the device is mounted. When the ghost image coincide with the real time image, the location of the next measurement point is determined based on the grid nodes and numbered points.

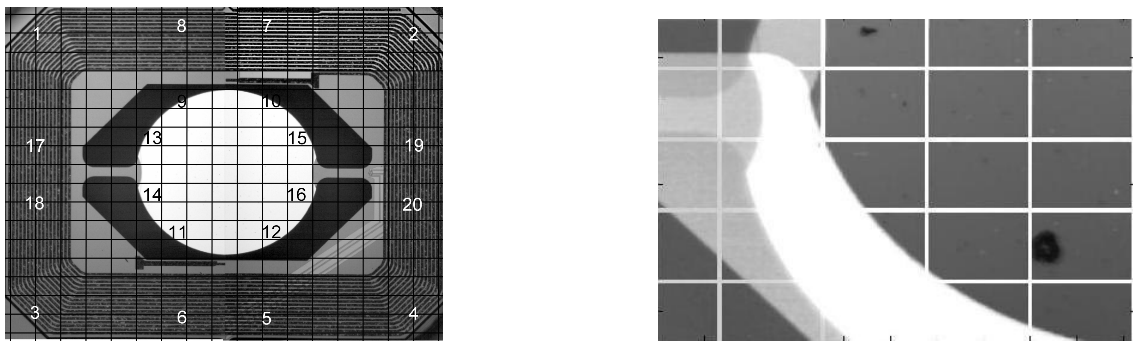

(a) (b)

Figure-2.5(a) Picture of the mirror with grids and measurement points. (b) The photo while matching the real image and transparent (ghost) image of the mirror.

When the next point for the following measurement is identified, the signal generator is driven with a sinusoidal input between 0-60 KHz range by using the LabView – GPIB interface (See Figure-2.2). This range is chosen due to the limitation of the NI 6034E DAQ card. Because the DAQ card has a sampling rate of 200 kilo Samples/second; the 60 KHz range is sufficient for making accurate dynamic measurements. The data that is collected by the laser interferometer (OFV-551) and the controller (OFV-5000) is transferred to a text file as frequency, amplitude and phase information using the Lab View interface program (See Figure-2.6). The Lab View program mainly uses lock-in amplifier toolkit which recovers the magnitude and phase of a sinusoidal signal partially or completely buried in broadband noise and eliminates the redundant data. As a result, more accurate phase and amplitude data can be collected from the measurements.

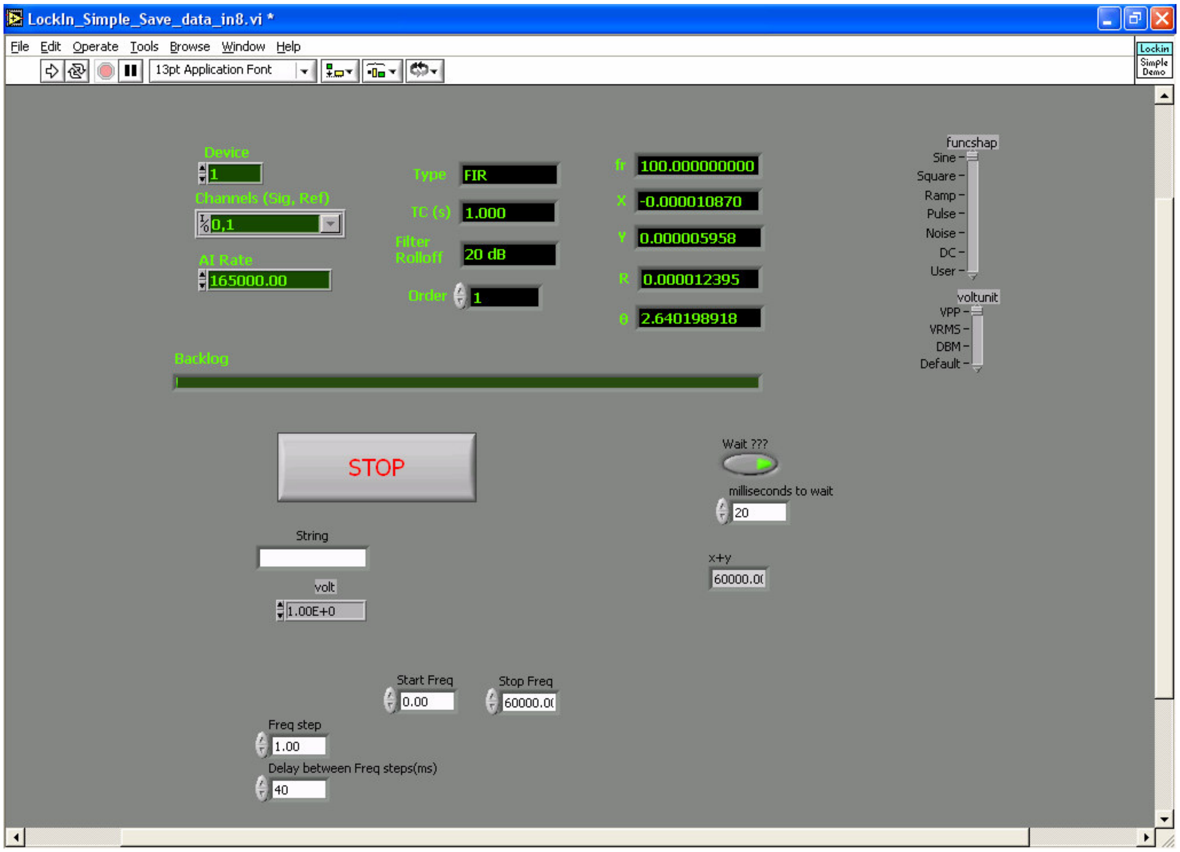

Figure-2.6 LabView program screen shot

For measuring the dynamic information completely, the device is operated in the 0-60 KHz range by directing the laser beam to the measurement points on the surface. At the end of this process, frequency response functions (FRF) (see Figure-2.7) that relate the excitation input to velocity output at various locations (Figure-2.5-a) on the micro structure are collected.

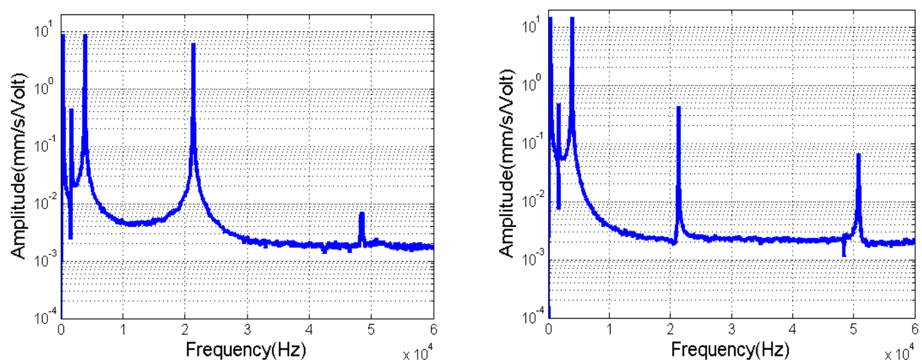

a) b)

Figure-2.7 An example that relates the excitation input to velocity output at points a) 11 and b) 3 (referred to Figure-2.5-a)

At the next step, the collected data between 0-60 KHz range is investigated and the frequency ranges which contain the main modal modes of the micro device are determined. The device is operated at these specific frequency ranges at low frequency increments like 0.5 Hz, 0.1 Hz or 1 Hz for more accurate and noise free measurements. The magnitude and phase data measured at the various collection points (Figure-2.5-a) is then transferred to the modal analysis software, ME'scope (see Figure-2.8).

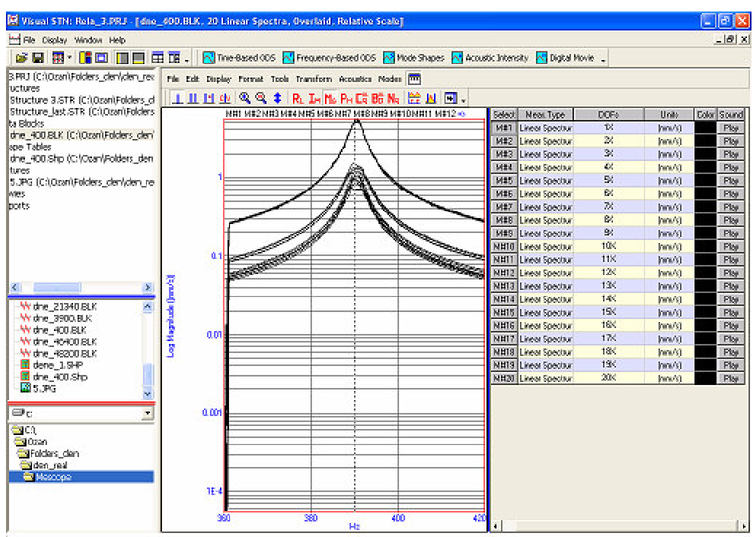

Figure-2.8 Screenshot of ME'scope for the transferred data between 360-420 Hz range.

After the data is transferred to the ME'scope software, the next step is building the geometric model of the micro mirror for visualizing the mode shapes. A real picture of the device is used to construct the 2D model at ME'scope (see Figure-2.9).

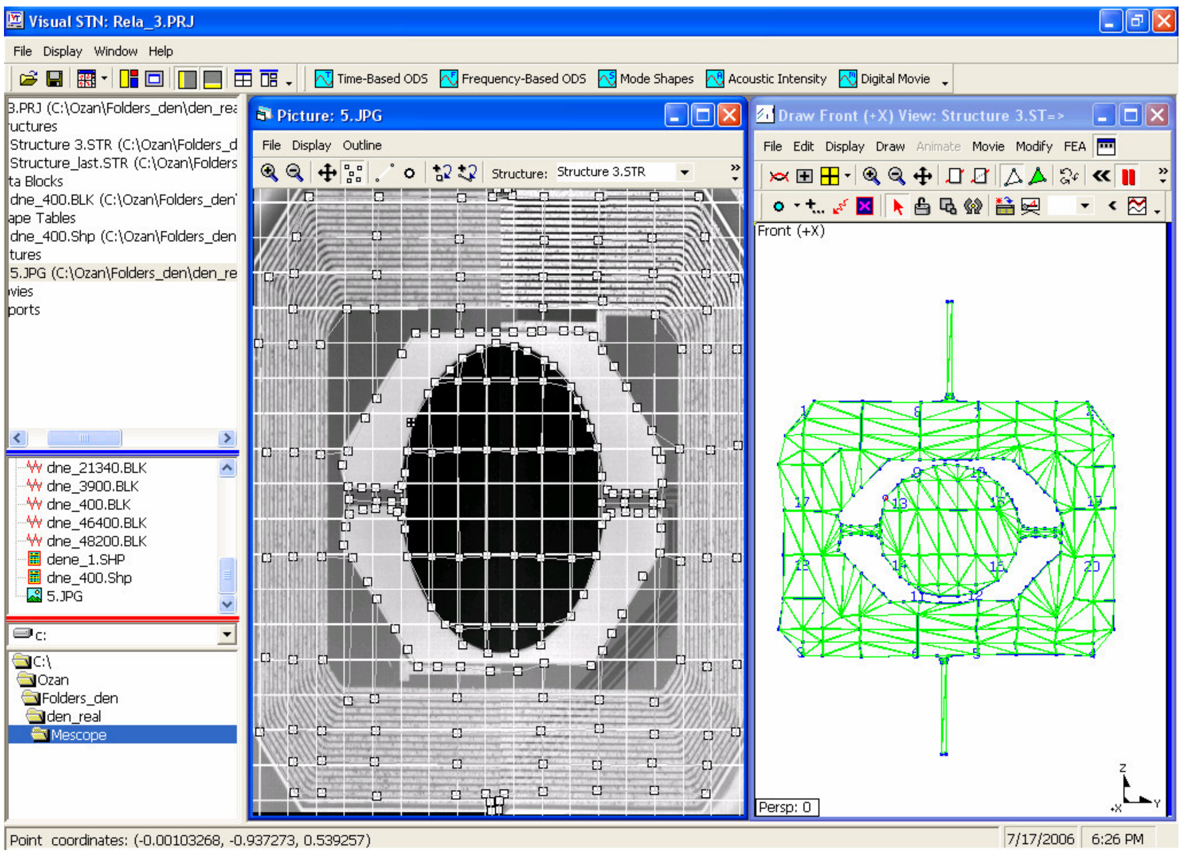

Figure-2.9 Screenshot of ME'scope while generating the experimental model

At the last step of ME'scope analysis, shape table of the complete modal analysis is created for overall system using both magnitude and phase information. The shape table shows the final results of the overall experimental modal analysis with mode shapes, natural frequencies and damping values of each mode (see Figure- 2.10).

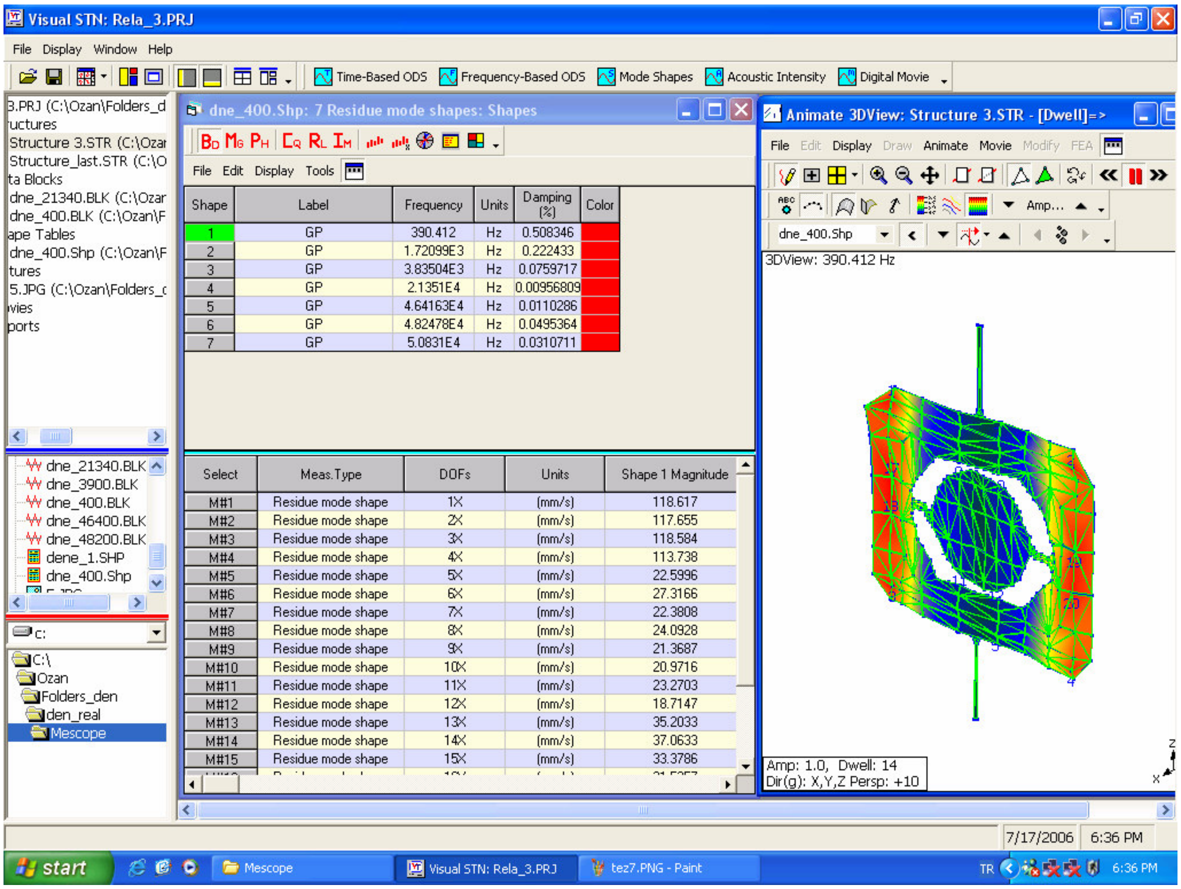

Figure-2.10 Shape table derived in ME'scope for complete experimental modal analysis of the MEMS micro mirror

ME'scope program estimates the modal parameters by curve fitting to a set of experimentally derived FRFs [26]. Curve fitting is a process of matching a parametric model of a FRF to a set of measurement data. The unknown parameters of the FRF model are modal frequency, modal damping & mode shape for each mode that is identified in the bandwidth of the measurements. Unknown modal parameters are extracted from the experimental data and ME'scope creates the FRF matrix in partial fraction form as in equation (2.1) in order to model the system completely;

$$\mathbf{H}(\boldsymbol{\omega}) = \sum_{k=1}^{modes}\left[\frac{\mathbf{R(k)}}{\mathbf{j\omega - p(k)}} + \frac{\mathbf{R^*(k)}}{\mathbf{j\omega - p^*(k)}}\right] \tag{2.1}$$

Where $\mathbf{H}(\boldsymbol{\omega})$ is *n* by *n* FRF matrix, $\mathbf{R(k)}$ is n by n residue matrix for the k^{th} mode, ω is the frequency variable (radians/second) and $p(k)$ is the pole location for the k^{th} mode and it is defined as:

$$p(k) = -\sigma(k) + j\omega_d(k) \tag{2.2}$$

where $\sigma(k)$ is the real part of the pole location and it is the modal damping for the k^{th} mode. $\omega_d(k)$ is the imaginary part of the pole location and it is the damped natural frequency for the k^{th} mode.

After the FRF matrix in Equation (2.1) is constructed, the percent of critical damping ($\zeta(k)$) for each mode can be calculated using the following equation:

$$\zeta(k) = \frac{\sigma(k)}{\sqrt{\omega(k)^2 + \sigma^2(k)}} \quad \text{in } (\%) \tag{2.3}$$

The values of percent critical damping for each mode can be seen at Table 2.1. In laterally moving micro scanners, damping is mainly caused by the viscous friction that originates from the air that surrounds the micro scanner. The calculated values in Table 2.1 are consistent with the estimates of the damping values obtained in previous studies [27-28].

2.2.3 Experimental Setup for In-Plane Measurements

In-plane vibration information is also required in order to have a complete 3D dynamic behavior of the micro devices. The testing system for measuring the out-of-plane motion was explained at sections 2.2.1 and 2.2.2, respectively. This section summarizes the technical specifications of the equipment that we use to build the modal testing system for in-plane measurements (See Fig-2.12 for details of the in-plane system).

2.2.3.1 Principle of Operation

The testing system for measuring the in-plane motion uses the stroboscopic illumination method (see Figure- 2.11). The stroboscopic illumination is mainly measuring the in-plane motions of periodically moving structures with stroboscopic machine vision. In this method; periodically moving structure, a light-emitting diode (LED) and a progressive scan camera must be combined and synchronized appropriately [29]. The system drives a digital camera to capture a sequence of the moving micro structure “frozen” by the strobe LED at different spaced phases. The procedure starts with operating the device at a specific frequency. Next, several images of the device are captured at a specific phase of the driving signal (see Figure- 2.11) through the use of instant lighting of the LED in camera exposure time. When the light is on, the image at the camera is captured and it represents the info at a specific phase of the driving signal [30]. After the images for a specific phase of the driving signal is taken, the phase difference between driving signal and the LED pulses is altered for having another set of images of the sinusoidal behavior of the moving device. When the above procedure is repeated and required images are taken for several phase differences, the sinusoidal motion of the micro device can be constructed by curve fitting to the displacements that are calculated from the images [29].

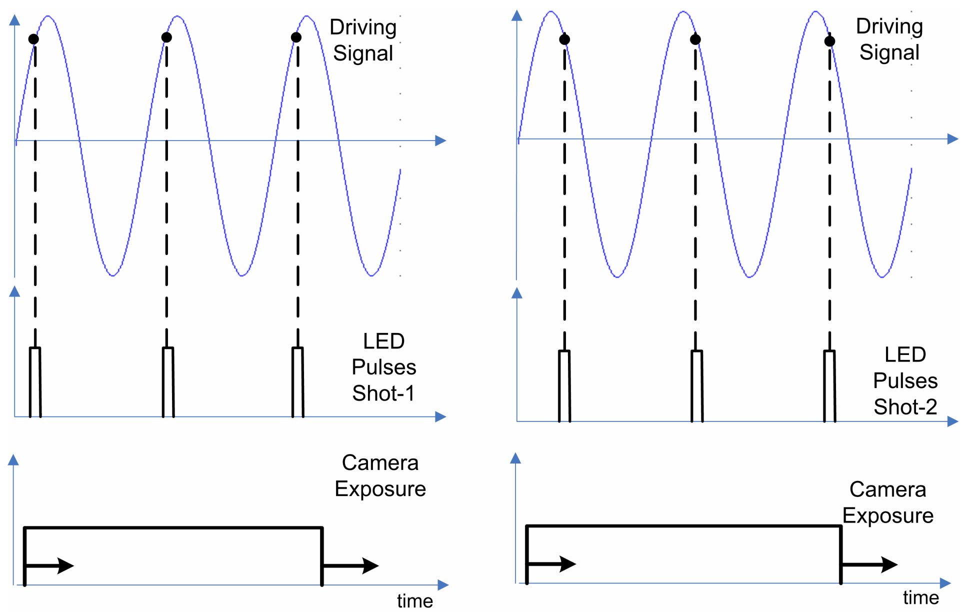

Figure- 2.11 Stroboscopic illumination phenomenon

2.2.3.2 In-Plane Motion Analysis Setup

The setup for out-of-plane vibration tests is used with some additional equipment in order to perform the in-plane measurements (Figure-2.12). The most important component of this setup is the LED due to its reliability as a light source that ensures constant illumination power of the strobe pulses. Because instant lighting is an important phenomenon for stroboscopic lighting; low turn on time with high luminosity is the main characteristic that the designer should have to consider while choosing the LED [29]. The LED that is chosen is a commercial Luxeon Star LXHL-MD1D high luminosity red LED which has a luminous flux of 44 lm at 350 mA and 100 ns turn-on time [31]. As a result 500 ns pulses can easily be obtained, which gives the opportunity measuring the motion of the micro structures that is operated up to 200 KHz by capturing 10 images at 10 different phases of one period [29].

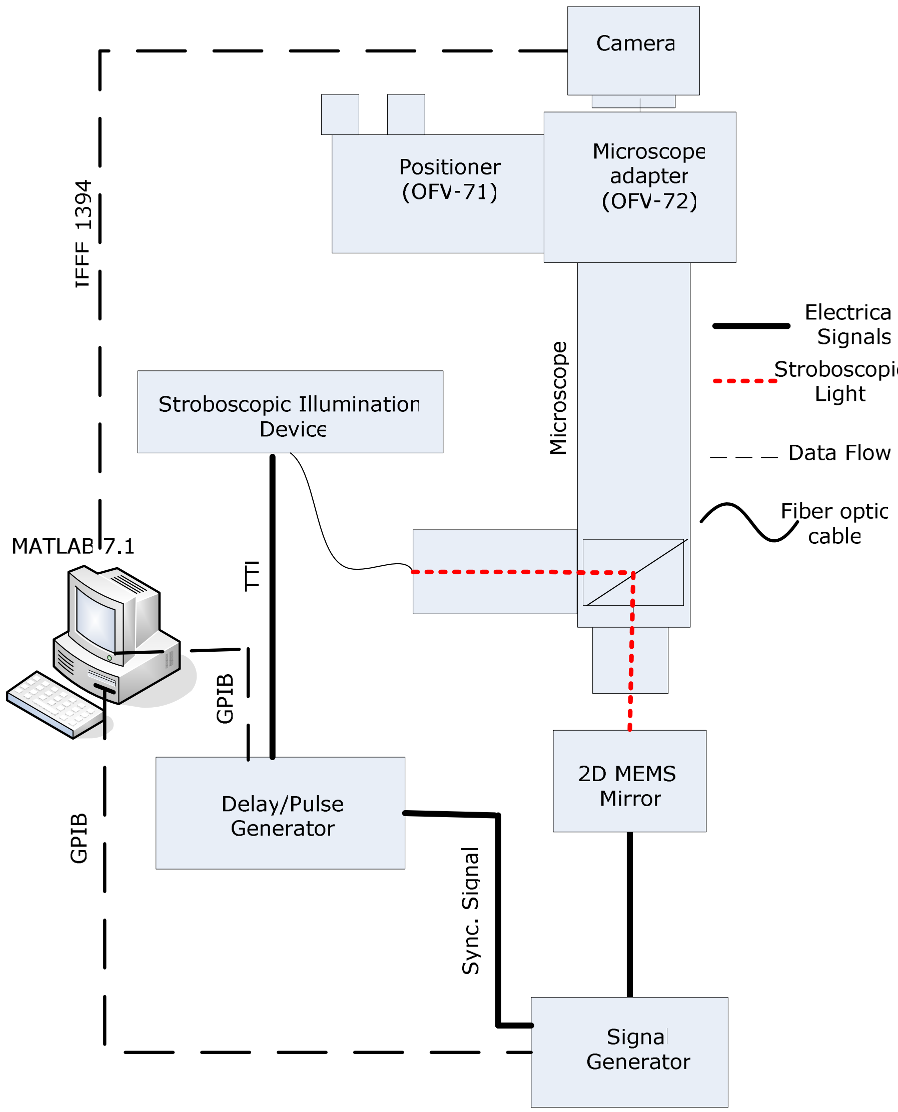

Figure-2.12 Setup for in-plane analysis

The driver is a "World Star Tech" LED driver that is used for modulating LED higher than 100 KHz. The driver can generate up to 300 mA constant current for driving the LED. It needs driving voltage between 3.5-5 Volts and a TTL signal as a control signal. The driving voltage is generated from a voltage source and the control signal is generated from a delay/pulse generator which is a Stanford Research Systems DG 535. The delay/pulse generator is synchronized with the signal generator in order to have sharp frozen images at required instant times.

A stroboscopic illumination module (SIM) is designed for combining all of the components used for stroboscopic lighting and also for adapting the components to the microscope system (Figure- 2.13). The components of this module are the lens, the LED, fiber optic cable, the heat sink and the driver. The lens, the LED and the fiber optic cable, are shrink fitted into a holder, which is manufactured from polyamide. Furthermore, the heat sink is used for the LED in order to make it lose heat while operating at an optimum temperature. The heat sink is glued to the LED and all the instruments are put in a compact box. The input for the SIM is the driving signal from the voltage source and the TTL signal from the delay/pulse generator. The output is the modulated light which is directed to the microscope system through the fiber cable.

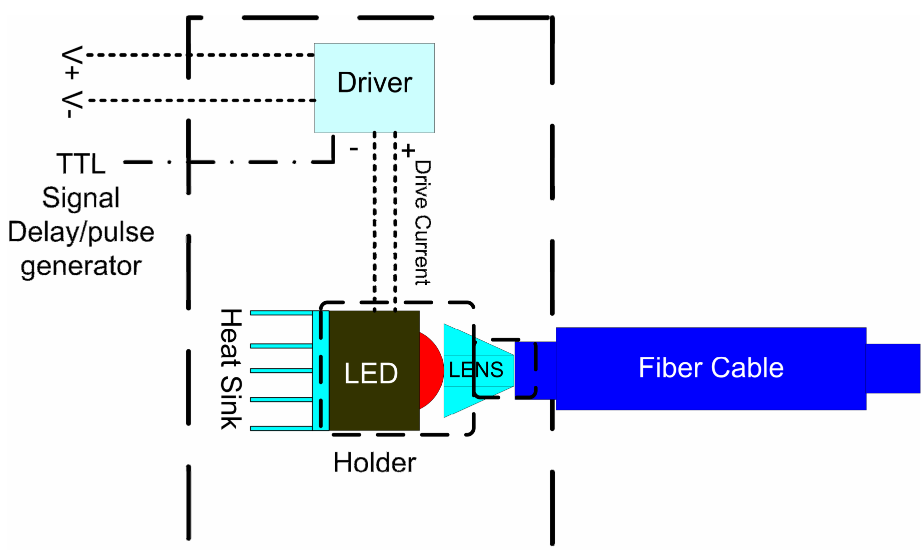

Figure-2.13 Inside view of stroboscopic illumination device

The camera pictures are image processed and the displacement of each measurement point is determined at various frequencies [29]. Unfortunately, this study is still in progress and the results are not currently available.

2.2.4 Results of the Experimental Analysis

The results for the out-of-plane modal analysis for two dimensional micro scanner is tabulated at Table-2.1. The mode descriptions are provided at the second row. The mode shape, modal frequency and percent of critical damping values are given at the third row.

First mode, at Table 2.1 is the torsional mode. At the torsional mode, the slow scan flexures (see Figure-1.4-(a)) rotate about the x-axis together with the overall structure. Second mode is the out-of-plane translation mode (in-phase). The slow scan flexures are bending and overall structure is translating along the z-axis. Third mode is the out-of-plane rocking mode (in-phase). The slow scan flexures and the rest of the structure rotate about the y-axis. Fourth mode is the out-of-plane rocking (out-of-phase) mode. The slow scan flexures are bending whereas fast scan flexures exhibit a torsional movement. At this mode the frame and the mirror rotate in opposite directions about y-axis. Fifth mode is the out-of-plane translation (out-of-phase) mode at which the slow scan flexures and the fast scan flexures are bending. The frame and the mirror translate along the z-axis separately in opposite directions. Sixth mode is the deflection mode for the outer frame. At this mode, the corners of the frame move independently.

Table- 2.1 Experimental modal analysis results

#	**1**	**2**	**3**	**4**	**5**	**6**
Mode Name	Torsional Mode	Out-of-plane Translation (In-phase)	Out-of-plane Rocking (In-phase)	Out-of-plane Rocking (Out-of-phase)	Out-of-plane Translation (Out-of-phase)	Outer Frame Deflection Mode
Experimental Mode shapes	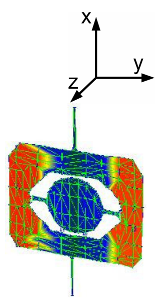 0.395 KHz $\zeta = \%$ **0.508**	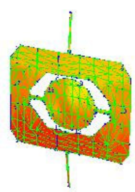 1.72 KHz $\zeta = \%$ **0.222**	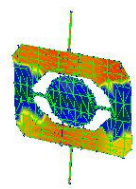 3.83 KHz $\zeta = \%$ **0.076**	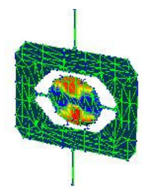 21.35 KHz $\zeta = \%$ **0.009**	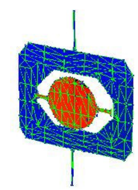 46.4 KHz $\zeta = \%$ **0.011**	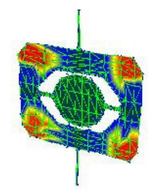 50.8 KHz $\zeta = \%$ **0.031**

2.3 Finite Element Analysis

The finite element model of the micro mirror was built using ANSYS software [32]. The FEM is used to extract the numerical eigenvalues and eigenvectors by conducting modal analysis. The geometric model of the mirror was generated in ANSYS using ANSYS Parametric Design Language (APDL) to parameterize the design variables. Design parameters can be changed easily and quickly using the APDL code. The APDL code was used for the sensitivity analysis while perturbing the design parameters which will be described in Chapter 4.

SOLID 95 solid elements were used in the 3D model generation of the micro scanner (see Figure-2.14). SOLID 95 can tolerate irregular shapes without as much loss of accuracy and they have compatible displacement shapes. Moreover, they are well suited to model curved boundaries. The SOLID 95 element is defined by 20 nodes having three degrees of freedom per node: translations in the nodal x, y, and z directions. Consequently, the element may have any spatial orientation. SOLID 95 has plasticity, creep, stress stiffening, large deflection, and large strain capabilities [32]. However, SOLID 95 does not have any rotational degrees of freedom. In the following studies, the input to our system is the disturbance torque acting on the mirror about the scanning axis. The output or equivalently the performance is defined as the variation of the mirror rotation angle under the effect of a disturbance torque. In order to obtain the relation between the input torque and the rotational displacement, SHELL 93 elements, which have rotational degrees of freedom, are attached to the SOLID 95 elements as a thin and low dense layer using the “contact pair” option in ANSYS. For this process, additional surfaces are created where the rotational motion is measured. Then, these surfaces are meshed by SHELL 93 elements. The important point here is that the density of these elements is very low relative to the main structure such that their effect does not change the modal characteristics of the structure. These elements are connected to the 3D model by using the “surface to surface contact” and multipoint constraint (MPC) algorithm options of ANSYS [32].

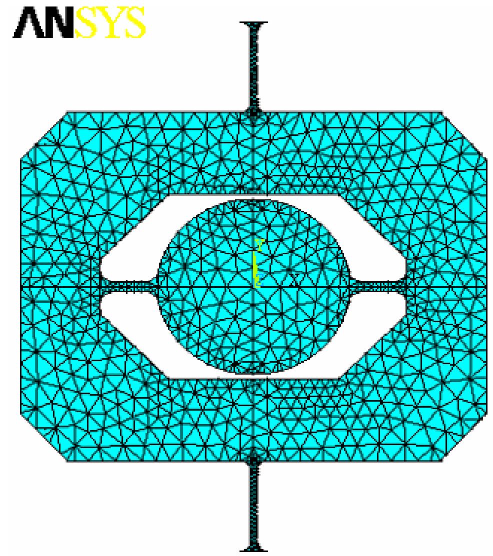

Figure-2.14 Finite element model of 2D micro mirror using 3D elements

The governing equation for the undamped free vibration of multi-degree of freedom system generated by Finite Element Analysis is [33]:

$$\mathbf{M}\ddot{\mathbf{x}}(\mathbf{t}) + \mathbf{K}\mathbf{x}(\mathbf{t}) = 0 \tag{2.4}$$

Where $\mathbf{M}$ is n by n mass matrix, $\mathbf{K}$ is n by n stiffness matrix, $\ddot{\mathbf{x}}(\mathbf{t})$ is n by 1 vector of accelerations, $\mathbf{x}(\mathbf{t})$ is n by 1 vector of displacements.

For a linear system, free vibrations will be harmonic of the form:

$$\mathbf{x}(\mathbf{t}) = \mathbf{\Phi} \sin(\Omega t + \phi) \tag{2.5}$$

Where $\mathbf{\Phi}$ is the vector of amplitudes of vibration, 'Ω' is the undamped frequency variable, ϕ is the phase angle between excitation and output signal and 't' is the time variable.

Differentiation of Equation (2.5) twice with respect to time leads to:

$$\ddot{\mathbf{x}}(\mathbf{t}) = -\Omega^2 \mathbf{\Phi} \sin(\Omega t + \phi) \tag{2.6}$$

Substituting Equations (2.5) and (2.6) into Equation (2.4) lead to

$$-\Omega^2 \mathbf{M\Phi sin}(\Omega \mathbf{t} + \phi) + \mathbf{K\Phi sin}(\Omega \mathbf{t} + \phi) = 0 \tag{2.7}$$

This leads to

$$-\Omega^2 \mathbf{M\Phi} + \mathbf{K\Phi} = 0 \tag{2.8}$$

Equation (2.8) can be considered as a system of homogenous equations in the vector of unknown amplitudes $\mathbf{\Phi}$. This equation can be written in the following form which is called the standard eigenvalue problem [33].

$$\left[\mathbf{K} - \Omega^2 \mathbf{M}\right]\mathbf{\Phi} = 0 \tag{2.9}$$

This equation has a nontrivial solution if and only if the coefficient matrix is singular, that is:

$$\left|\mathbf{K - \Omega^2 M}\right| = 0 \tag{2.10}$$

This equation is called the characteristic equation and the solution of this equation leads to a polynomial order *n* with the variable Ω^2. The roots of this polynomial are denoted as $\Omega_i^{\,2}$, where 'i' represents the number of the roots from 1 to *n*, called eigenvalues. The square roots of the eigenvalues (Ω_i) are called the natural frequencies of the undamped multi-degree of freedom system. Thus a system with *n* degrees of freedom has *n* natural frequencies.

Associated with each characteristic value Ω_i, there is a vector called the eigenvector $\mathbf{\Phi_i}$ (sometimes referred to as the i^{th} mode shape of vibration) which can be obtained by using Equation (2.9).

ANSYS modal analysis results, which are eigenvalues (natural frequencies) and eigenvectors (mode shapes), are used to characterize the vibrational behavior of the mirror. The model predictions are compared with the experimental results to correct and improve the finite element model.

2.3.1 Results of Finite Element Analysis

The results of finite element modal analysis are shown at Table 2.2. There are four additional in-plane modes when compared with the previous experimental results. One of the new modes is the 3rd mode which is called as in-plane translation mode. At this mode, the structure moves along the y-axis while the slow scan flexures are bending. The other one is the 5th mode which is the in-plane rocking mode and at this mode the structure rotates about the z-axis.

Table - 2.2 Results of the finite element modal analysis

#	Mode Description	Mode Shapes and Frequencies	#	Mode Description	Mode Shapes and Frequencies
1	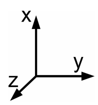 Torsional	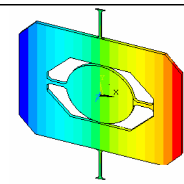 0.39 KHz	6	Out-of-plane rocking (Out-of-Phase)	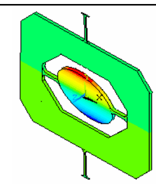 21.38 KHz
2	Out-of-plane translation (In-Phase)	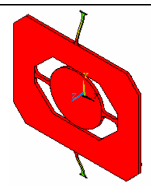 2.1 KHz	7	Out-of-plane translation (Out-of-Phase)	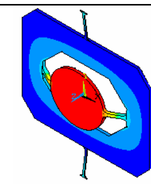 47.24 KHz
3	In-plane translation	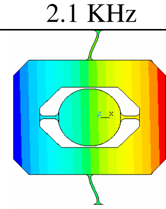 4.4 KHz	8	Axial translation (In-Phase)	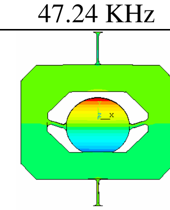 50.7 KHz
4	Out-of-plane rocking (In-Phase)	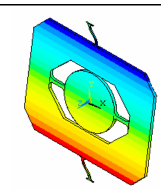 4.5 KHz	9	Outer Frame Deflection Mode	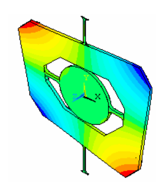 58.9 KHz
5	In-plane rocking	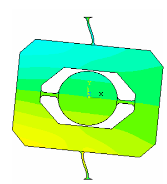 5.0 KHz	10	Axial translation (Out-of-Phase)	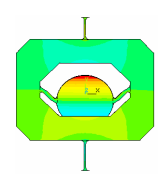 86.8 KHz

The other new mode is called axial translation (in-phase). At this mode, the slow scan flexures move along the x-axis and the fast scan flexures are bending. Both the frame and the mirror move along the x-axis in the same direction. The last in-plane mode is the axial translation (out-of-phase). This mode is the same as the axial translation (in-phase) mode but at this mode the frame and mirror move along the x-axis at opposite directions.

2.4 Analytical Formulations

The separation of critical vibration modes and high frequency requirements are critical for 2D microscanners. During the initial design stage before the FEM is constructed, the designer can utilize analytical formulations to predict the modal frequencies of the system.

The modal frequencies of the 2-D micro scanner mirror were determined using the formulations that are driven for the 1-D micro scanner [34] (see Figure-2.15). The analytical formulations used to calculate the inertia properties and stiffness constants are tabulated in Table 2.3 and 2.4. The Saint Venant Theory is used for the derivation of the torsional stiffness and the Euler-Bernoulli beam theory is used for the bending mode stiffness values of the flexures [34]. Appropriate inertia and stiffness corrections are made for the 2-D micro scanner and the out-of-plane and in-plane rigid body modes are predicted assuming a first order system which has single mass and single stiffness (see Figure-2.16).

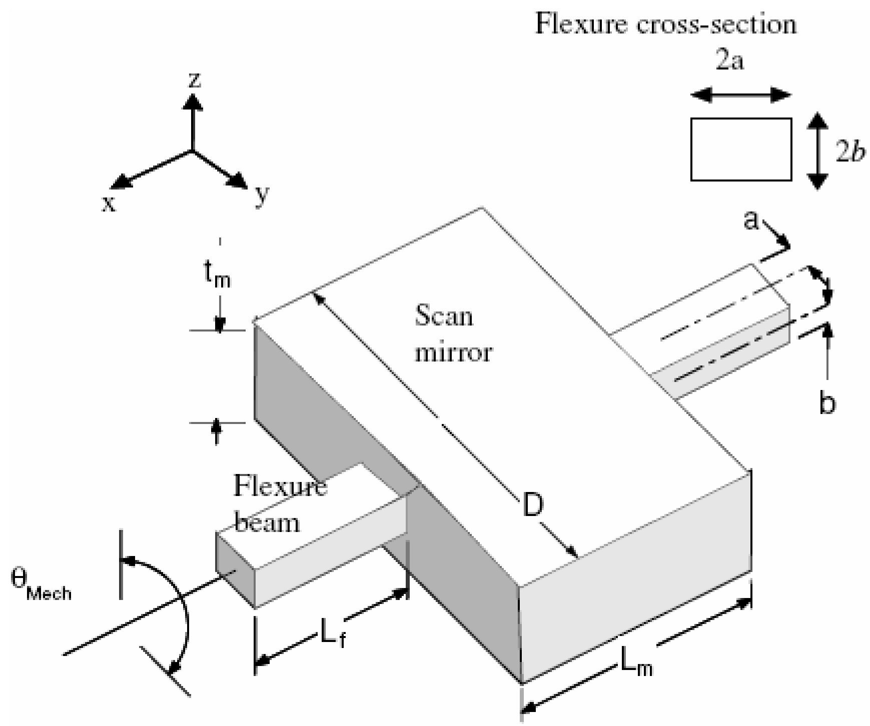

Figure-2.15 One dimensional torsional resonant scan mirror suspended with two flexure beams that are fixed at the ends. The inset shows the critical dimensions and coordinate axis that are used for driving the formulae at Table-2.3 [34]

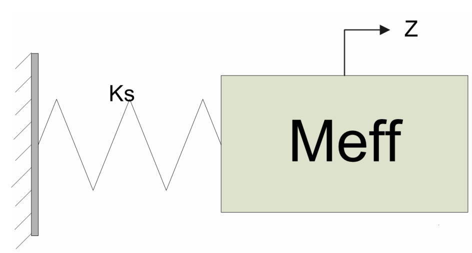

Figure- 2.16 One mass one spring system

Table-2.3 Parameters used for calculating the theoretical modal frequencies of the 1-D micro scanner [34]

	Effective mass (M_{eff}) / **Mass moment of inertia** (J_{eff})	**Spring Constant** (K_s)
1. Torsion	$J_{eff} = J_{m,xx} + (2/3)J_{f,xx}$ $J_{f,xx} = \frac{1}{3}M_f(a^2 + b^2)$ $M_f = 4abL_f$	$K_s = \frac{2GK}{L_f}; \mu = \sqrt{G_{xz}/G_{xy}}$ where GK is given by $GK = \begin{cases} (ab^3G_{xy})\left[5.33 - 3.36\frac{b}{a\mu}\left(1 - \frac{b^4}{12a^4\mu^4}\right)\right] & a\mu \ge b \\ (ba^3G_{xz})\left[5.33 - 3.36\frac{a\mu}{b}\left(1 - \frac{a^4\mu^4}{12b^4}\right)\right] & a\mu \le b \end{cases}$
2.Out-of-plane sliding	$M_{eff} = M_m + \frac{26}{35}M_f$	$K_s = \frac{24E_xI_{yy}}{L_f^3}; \quad I_{yy} = \frac{4}{3}ab^3$
3. In-plane sliding	$M_{eff} = M_m + \frac{26}{35}M_f$	$K_s = \frac{24E_xI_{zz}}{L_f^3}; \quad I_{zz} = \frac{4}{3}ba^3$
4. Out-of plane rocking	$J_{eff} = J_{m,yy} + 2J_f$ $J_f = M_f(0.0095L_f^2$ $+ 0.052L_fL_m + 0.0929L_m^2)$	$K_s = \frac{E_xI_{yy}\left(2 + 6\left(1 + \frac{L_m}{L_f}\right)^2\right)}{L_f}$
5. In-plane rocking	$J_{eff} = J_{m,zz} + 2J_f$	$K_s = \frac{E_xI_{zz}\left(2 + 6\left(1 + \frac{L_m}{L_f}\right)^2\right)}{L_f}$

Table -2.4 Mass and Mass moment of inertia for different mirror shapes [34]

	M_m	$J_{m,xx}$	$J_{m,yy}$	$J_{m,zz}$
Rectangular Mirror	$\rho L_m D t_m$	$\frac{M_m}{12}\left(D^2 + t_m^2\right)$	$\frac{M_m}{12}\left(L_m^2 + t_m^2\right)$	$\frac{M_m}{12}\left(D^2 + L_m^2\right)$
Elliptical Mirror	$\frac{\pi}{4}\rho L_m D t_m$	$\frac{M_m}{12}\left(\frac{3}{4}D^2 + t_m^2\right)$	$\frac{M_m}{12}\left(\frac{3}{4}L_m^2 + t_m^2\right)$	$\frac{M_m}{16}\left(D^2 + L_m^2\right)$

As an example, the natural frequency for the out-of-plane sliding mode, which is translation of the mirror along the z-axis, with natural frequency of Ω can be calculated as:

$$\frac{d^2z}{dt^2} + \Omega^2 z = 0 \tag{2.11}$$

$$\Omega = 2\pi f = \sqrt{K_s / M_{eff}} \tag{2.12}$$

The elliptical mirror and the outer frame moves in-phase at the torsional, out-of-plane translation (in-phase) and out-of-plane rocking (in-phase) modes (see Table 2.1 and 2.2 for the definition of the mode shapes). For these modes, the overall system can be considered as 1D rectangular micro mirror except that the inertia of the space between the mirror and the frame must be subtracted from the overall effective mass and mass moment of inertia of a rectangular mirror with the same size. The other two modes are; out-of-plane rocking (out-of-phase) and out-of-plane sliding (out-of-phase), at which the mirror and the outer frame move separately (see Figure-2.17). At these modes, the system can be modeled as two-mass system which has two unequal bodies and two unequal springs (see Figure-2.18). Two unequal bodies stand for the inertia for the outer frame and the inertia of the mirror. Two unequal springs stand for the stiffness values of the fast scan and slow scan flexures. The theoretical calculation of the natural frequency that represents the two-body system can be found at Blevins [35]. The formula used for this system is:

$$\Omega = \frac{1}{2^{3/2}\pi}\left\{\frac{Ks1}{Meff1} + \frac{Ks2}{Meff1} + \frac{Ks2}{Meff2} \mp \left[\left(\frac{Ks1}{Meff1} + \frac{Ks2}{Meff1} + \frac{Ks2}{Meff2}\right)^2 - \frac{4Ks1Ks2}{Meff1Meff2}\right]^{1/2}\right\}^{1/2} \tag{2.13}$$

As it can be seen from Equation (2.13), the system has two natural frequencies where the two bodies move in the same (in-phase) and opposite (out-of-phase) directions. The modal frequencies for the out-of-plane rocking (out-of-phase) and out-of-plane translation (out-of-phase) modes (see Table 2.1) can be achieved analytically using Equation (2.13). The 6th mode, which is called the deflection mode in Table 2.1, is the plate deflection mode and it is difficult to predict using the given analytical formulations.

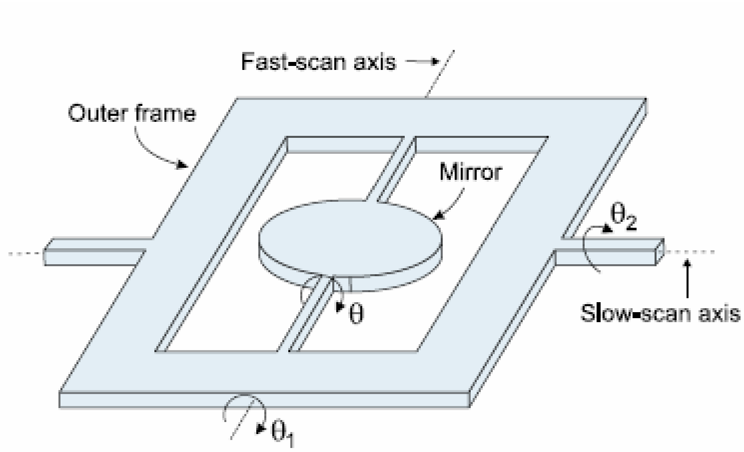

Figure-2.17 Schematic of the outer frame and the mirror [12]

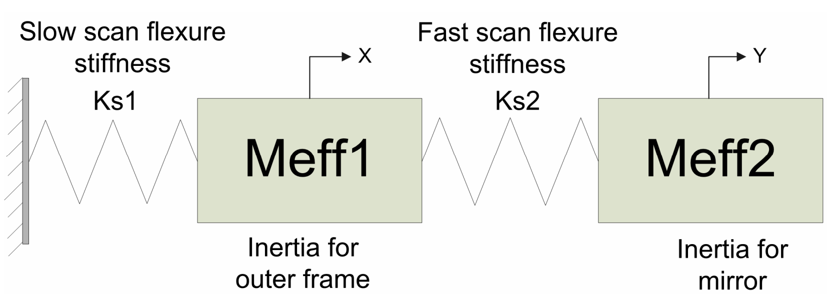

Figure-2.18 Two mass and two spring system

2.4.1 Results of Theoretical Analysis

Theoretical frequency calculation results for different mode shapes are given at Table 2.5. The mode descriptions of the modal frequencies can be found at Sections 2.2.4 and 2.3.1. The comparison of theoretical calculations with the FEM and experimental results will be given in Chapter 3.

Table 2.5 Theoretical frequency results for Bimag micro scanner mirror

Modes	Theoretical Frequencies (Hz)
Torsional Mode	347
Out-of-plane translation	1937
In-plane translation	3725
Out-of-plane rocking (in-phase)	4233
In-plane rocking	4855
Out-of-plane rocking (out-of-phase)	18000
Out-of-plane translation (out-of-phase)	64558

Chapter 3

VALIDATION OF THE FEM AND STATE SPACE REPRESENTATION OF THE 2D SCANNER

3.1 Introduction

This chapter compares the FEM and the experimental analyses' results. The accuracy of the FEM vas investigated and it was used for further design studies in Chapter 4. The frequencies calculated by the analytical formulations are also compared with the experimental results and the accuracy of the analytical formulations in predicting the natural frequencies of the micro scanner is discussed. This chapter also summarizes the theoretical background in order to build the state space representation of the system after the FEM is validated.

3.2 Comparison of Experimental, Numerical and Analytical Results

Table 3.1 summarizes the experimental and finite element analysis results (see 3rd and 4th rows of Table 3.1). The 5th row of Table 3.1 shows the modal frequencies calculated by the analytical formulations. Due to the fact that, the current experimental system is limited to the out-of plane velocity measurements, the resultant in-plane and coupled modes are not considered for comparison

Table 3.1 Comparison chart for modal analysis results

#	1	2	3	4	5	6
Mode Description	Torsional Mode	Out-of-plane Translation (In-phase)	Out-of-plane rocking (In-Phase)	Out-of-plane rocking (Out-of-phase)	Out-of-plane Translation (Out-of-phase)	Outer Frame Deflection Mode
Experimental Mode shapes	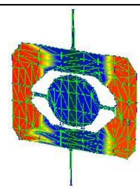 0.395 KHz	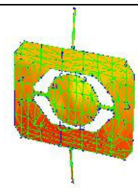 1.72 KHz	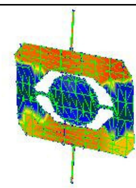 3.83 KHz	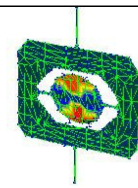 21.35 KHz	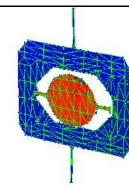 46.4 KHz	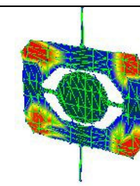 50.8 KHz
FEM Mode shapes	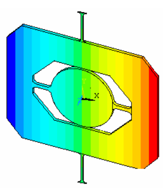 0.39 KHz	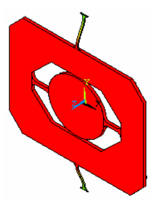 2.1 KHz	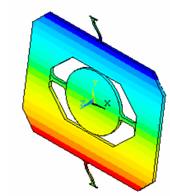 4.5 KHz	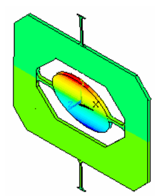 21.38 KHz	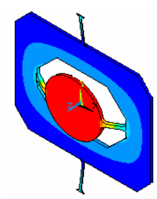 47.24 KHz	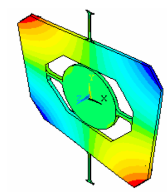 58.9 KHz
Theoretical frequencies	0.347 KHz	1.94 KHz	4.23 KHz	18 KHz	64.5 KHz	--------

.

In order to quantify the differences between the predicted and experimental results, we defined an error function assuming that the experimental results represent the truth. The percent error relative to the experimental frequencies are calculated by the following Equation (3.1) and tabulated at Table 3.2.

$$\% \text{ error} = 100\left[\frac{f_{fem} - f_{exp}}{f_{exp}}\right] \quad \text{or} \quad \% \text{ error} = 100\left[\frac{f_a - f_{exp}}{f_{exp}}\right] \tag{3.1}$$

Where 'f_{exp}' is the experimental frequency for the mode shape, 'f_a' is the analytical frequency for the mode shape and 'f_{fem}'is the finite element modal analysis frequency.

Table-3.2 Table for error values calculated according to Equation (3.1)

Mode Number	% error FEM	% error Analytical
1	-1.2	-12
2	22	13
3	17.5	10
4	0.1	-16
5	1.8	39
6	16	------

The differences between the FEM predictions and experimental results are mainly originated from the inaccurate modeling assumptions. The finite element model predicts the 1st, 4th and 5th mode shapes and frequencies very accurately but the natural frequencies are slightly different for the 2nd, 3rd and 6th modes. Since 2nd and 3rd modes are bending modes for slow scan flexure it is believed that this discrepancy is caused by the modeling imperfections in the slow scan flexure dimensions (see Figure-3.1). The 6th mode is also difficult to predict since it requires precise knowledge of the outer frame dimensions and mass properties. Although we assumed that experimental results represent the truth, they may be affected by the environmental factors such as humidity, dust and temperature. Micro systems may be affected due to their low mass properties that change from microgram to picogram. For instance, water droplets by humidity and dust particles may stick on the micro structure during the experimental analysis. These kinds of effects may increase the effective inertia and effective mass values of the micro system which eventually generates a shift in the natural frequencies according to the Equation (2.12). Moreover, temperature changes at the experimental environment is another factor that needs to be considered. The temperature changes may cause expansion or contraction of the micro mirror which also causes the change in effective mass and inertia of the micro system. As a result, small disturbances which are insignificant in 'macro' world can significantly affect the dynamic performance of a micro system and may lead to a change in the natural frequencies. Improvements and corrections are required both in the modeling and experimental area in order to have a better match between the measured and simulation results.

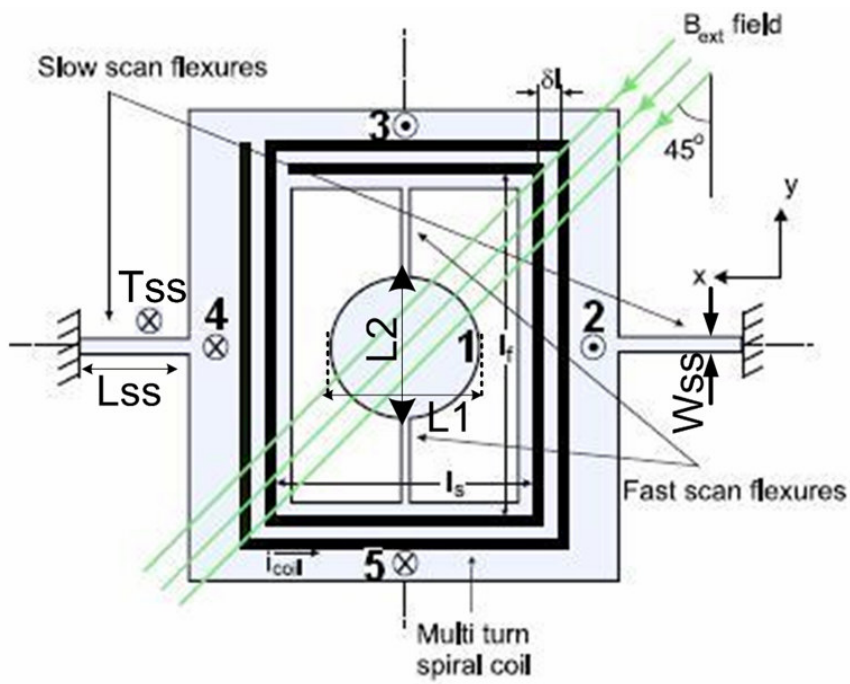

Figure-3.1 Numbered Schematic of Bimag Scanner mirror

When the percent error for the analytical formulations is investigated, it can be seen that the modal frequencies for the first four modes are in reasonable range. However the 5th mode's frequency does not match the experimental results. This discrepancy can be explained by changing boundary conditions, which are uncontrolled deflections, when the mirror and the outer frame move separately. Due to these uncontrolled boundary conditions, the flexure stiffness can not be calculated using the formulations given in Table 2.3 and 2.4. Also, the imperfections in mass and inertia calculations may cause the discrepancies between the experimental and analytical results. Moreover, we believe that there is an error accumulation in predicting the frequencies of 4th and 5th modes. At these modes the mirror and the outer frame move out-of-phase where the modeling inaccuracies in both flexures (see Figure- 3.1) contribute to the error accumulation.

3.3 State Space Modeling

State space representation is a matrix based formulation of a linear system equation of motion by utilizing a set of variables, known as state variables [36]. With the state space representation, first order system models can be modeled using a matrix notation. The time domain state space representation lends itself easily to computer simulations and dynamic analysis [36].The concept of state space representation can be explained based on a mass-spring damper system which is shown on Figure-3.2.

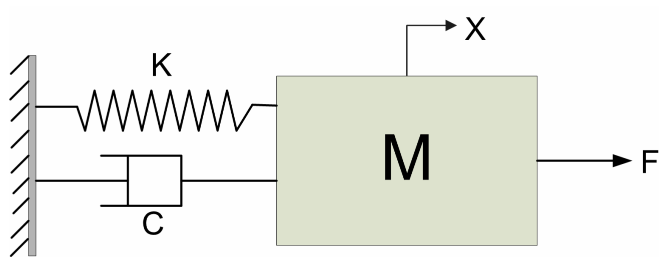

Figure-3.2 Mass-Spring-Damper system

The equation of motion of a single mass, spring, damper system is:

$$m\ddot{x} + c\dot{x} + kx = F \tag{3.2}$$

Where 'm' is the mass, 'c' is damping coefficient, 'k' is spring constant and 'F' is the force applied on the mass. By describing new set of variables we can change the equation of motion to a set of first order equations in a matrix notation.

$$\begin{aligned} x_1 &= x \\ x_2 &= \dot{x} \end{aligned} \tag{3.3}$$

The differential equation of motion can be written in the form:

$$\begin{aligned} \dot{x}_1 &= x_2 \\ \dot{x}_2 &= -\frac{c}{m} - \frac{k}{m} + \frac{F}{m} \end{aligned} \tag{3.4}$$

A second order equation of motion is now written in the form of two first order differential equations which are easier to solve. For systems having *n* degrees of freedom, '*n*' 2^{nd} order differential equations will represent the system and the state-space representation of this system will be in the form of '*2n*' differential equations of first order [9]. If we write the system in matrix form:

$$\begin{bmatrix} \dot{x}_1 \\ \dot{x}_2 \end{bmatrix} = \begin{bmatrix} 0 & 1 \\ -\frac{k}{m} & -\frac{c}{m} \end{bmatrix} \begin{bmatrix} x_1 \\ x_2 \end{bmatrix} + \begin{bmatrix} 0 \\ \frac{F}{m} \end{bmatrix}$$

$$\mathbf{A}= \begin{bmatrix} 0 & 1 \\ -\frac{k}{m} & -\frac{c}{m} \end{bmatrix} \qquad \mathbf{B}= \begin{bmatrix} 0 \\ \frac{F}{m} \end{bmatrix} \tag{3.5}$$

Where Equation (3.5) is called as 'state differential equation'.

The outputs of the linear mass-spring-damper system can be related to the state variables by:

$$y = \mathbf{C} \begin{bmatrix} x_1 \\ x_2 \end{bmatrix} + \mathbf{Du(t)} \tag{3.6}$$

Where **C** is the output matrix which relates state and output variables and **D** is the direct transformation matrix which directly affects the output regardless of the states.

For continuous systems that have several modes, the system can be modeled as a combination of second order systems for each mode contribution:

$$\mathbf{A}=\begin{bmatrix} 0 & 1 & 0 & 0 & \cdots\cdots & \cdots\cdots \\ -\frac{k_1}{m_1} & -\frac{c_1}{m_1} & 0 & 0 & \cdots\cdots & \cdots\cdots \\ 0 & 0 & 0 & 1 & \cdots\cdots & \cdots\cdots \\ 0 & 0 & -\frac{k_2}{m_2} & -\frac{c_2}{m_2} & \cdots\cdots & \cdots\cdots \\ \cdots\cdots & \cdots\cdots & \cdots\cdots & \cdots\cdots & \cdots\cdots & \cdots\cdots \\ \cdots\cdots & \cdots\cdots & \cdots\cdots & \cdots\cdots & \cdots\cdots & \cdots\cdots \end{bmatrix}. \quad \mathbf{B}=\begin{bmatrix} 0 \\ 1 \\ 0 \\ 0 \\ \cdots \\ \cdots. \end{bmatrix}$$

$$\mathbf{C}=\begin{bmatrix} 0 & 0 & 1 & 0 & \cdots\cdots & \cdots\cdots \end{bmatrix} \qquad \mathbf{D}=[0] \tag{3.7}$$

Where **A** matrix is a combination of each individual modal mode which has its own stiffness and effective mass. According to the Equation (3.2) k_1 and k_2 are first and second natural modes' stiffness values and m_1 and m_2 are the modal masses for the corresponding mode shapes. For instance, in the 2D micro scanner mirror case, the first mode corresponds to the torsional mode that has its own torsional stiffness which comes from the slow scan flexure effective torsional stiffness and modal mass corresponds to the effective inertia of the overall system for torsional movement. For **B** and **C** matrices, the placement of ones and zeros are determined by the input/output location. The ones of **B** matrix are assigned for the states where the inputs are applied. For the **C** matrix ones are assigned for the states where the outputs are measured.

Stiffness and inertia terms are the physical system parameters that depend on the design variables of the 2D mirror. The equations of motion written for the physical system parameters in physical coordinates are coupled equations and have to be solved simultaneously. Another coordinate system which is called 'principal coordinate system' can be defined in order to uncouple the equations of motion. 'Principal coordinate system' can be defined by using the system eigenvectors, which are the modal analysis results [37].

The 'physical parameters' can be changed to the 'principal parameters' by the following way:

$$\mathbf{\Phi}^{\mathbf{T}}\mathbf{M}\mathbf{\Phi}\ddot{\mathbf{x}}_{\mathbf{p}} + \mathbf{\Phi}^{\mathbf{T}}\mathbf{C}\mathbf{\Phi}\dot{\mathbf{x}}_{\mathbf{p}} + \mathbf{\Phi}^{\mathbf{T}}\mathbf{K}\mathbf{\Phi}\mathbf{x}_{\mathbf{p}} = 0 \tag{3.8}$$

Where Equation (3.8) is the unforced equation of motion of an '*n*' DOF system, '$\mathbf{\Phi}$' is combination of all eigenvectors calculated for all eigenvalues and '$\mathbf{x}_{\mathbf{p}}$' is the vector of principal coordinates. '**M**', '**C**' and '**K**' are the mass, damping and stiffness matrices in physical coordinates respectively. After the matrix multiplication is done at Equation (3.8), Equation (3.9) is obtained as:

$$\mathbf{M}_{\mathbf{p}}\ddot{\mathbf{x}}_{\mathbf{p}} + \mathbf{C}_{\mathbf{p}}\dot{\mathbf{x}}_{\mathbf{p}} + \mathbf{K}_{\mathbf{p}}\mathbf{x}_{\mathbf{p}} = 0 \tag{3.9}$$

Where '$\mathbf{M}_{\mathbf{p}}$', '$\mathbf{C}_{\mathbf{p}}$' and '$\mathbf{K}_{\mathbf{p}}$' are the mass, damping and stiffness matrices in principal coordinates respectively. Equation (3.9) can then be written as '*n'* uncoupled differential equations using modal parameters:

$$\ddot{x}_i + 2\zeta_i\omega_i\dot{x}_i + \omega_i^{\,2}x = 0 \tag{3.10}$$

Where 'ζ_i' is modal damping factor and ω_i is the natural frequency for the i^{th} mode shape. Using these modal parameters the state space equation can be written as [37]:

$$\mathbf{A_p} = \begin{bmatrix} 0 & 1 & 0 & 0 & \cdots & \cdots \\ -\omega_1^{\ 2} & -2\zeta_1\omega_1 & 0 & 0 & \cdots & \cdots \\ 0 & 0 & 0 & 1 & \cdots & \cdots \\ 0 & 0 & -\omega_2^{\ 2} & -2\zeta_2\omega_2 & \cdots & \cdots \\ \cdots & \cdots & \cdots & \cdots & \cdots & \cdots \\ \cdots & \cdots & \cdots & \cdots & \cdots & \cdots \end{bmatrix} \cdot \quad \mathbf{B_p} = \mathbf{\Phi}^{T} \begin{bmatrix} 0 \\ 1 \\ 0 \\ 0 \\ ... \\ .... \end{bmatrix}$$

$$\mathbf{C_p} = \mathbf{\Phi}[0 \quad 0 \quad 1 \quad 0 \quad ..... \quad .....] \qquad \mathbf{D_p} = [0] \qquad (3.11)$$

'$\mathbf{\Phi}$' is modal transformation matrix obtained from ANSYS modal analyses results. $\mathbf{A_p}$, $\mathbf{B_p}$, $\mathbf{C_p}$ and $\mathbf{D_p}$ are state space matrices in principal coordinates.

3.4 State Space Model Generation of 2D Micro Scanner Mirror

The state space model of the 2D micro scanner mirror is generated using the method that is described in Section 3.3. The micro scanner mirror chosen for the case study is designed for operation at its torsional mode and out-of-plane rocking (out-of-phase) modes which are 1st and 4th modes on Table 3.1. Consequently, design considerations and input-output relationships are chosen accordingly. In this manner, state space representation of the 2D microscanner is built such that inputs are applied at points 2&3 and outputs are measured at points 1&3 (see Figure-3.1). Resultant torques generated by the Lorent'z forces are applied at the input locations and rotational displacements of the output locations are measured. The input matrix $\mathbf{B_M}$ and output matrix $\mathbf{C_M}$ are built such that the required input-output relations are satisfied.

First ten mode shapes that are extracted from ANSYS modal analysis results which are eigenvectors and eigenvalues (see Table 2.2 for finite element analyses results) are taken into consideration for generation of the $\mathbf{A_M}$ matrix. The eigenvalues are the modal frequencies for each mode shape and the ζ values are obtained from the experimental modal analyses results (see Table 2.1 Experimental analyses results) for each mode contribution.

$\mathbf{D_M}$ matrix which is called 'direct transmission matrix' is taken as zero matrix because there is no other external source that directly affects the main output of the system. As a result, the state space representation is written in the following form:

$$\begin{aligned} \dot{\mathbf{x}}(t) &= \mathbf{A}_M \mathbf{x}(t) + \mathbf{B}_M \mathbf{u}(t) \\ \mathbf{y}(t) &= \mathbf{C}_M \mathbf{x}(t) \end{aligned} \tag{3.12}$$

Where $\mathbf{A}_M$, $\mathbf{B}_M$ and $\mathbf{C}_M$ are state space representation matrices in principal coordinates for the 2D micro mirror.

After the state space representation of the system is completed, the Bode plots, which are magnitude versus frequency diagrams are plotted in order to obtain the transfer functions for related input/output configurations. The Bode plots for corresponding input/output relations can be seen in Figure-3.3.

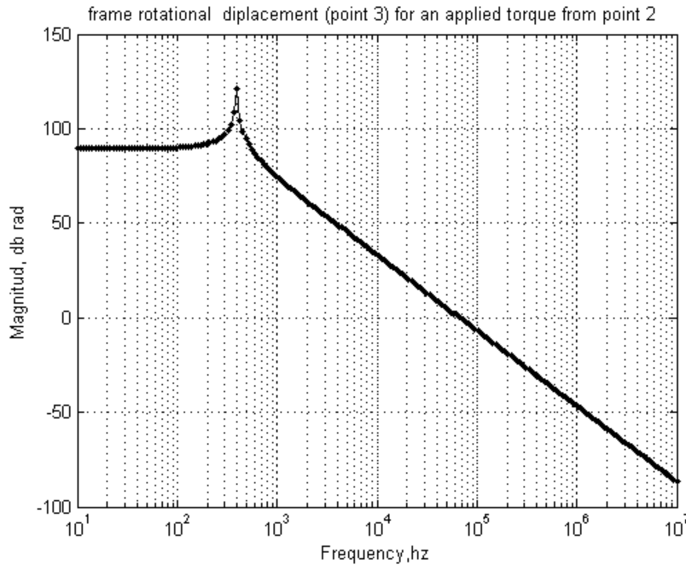

(a)

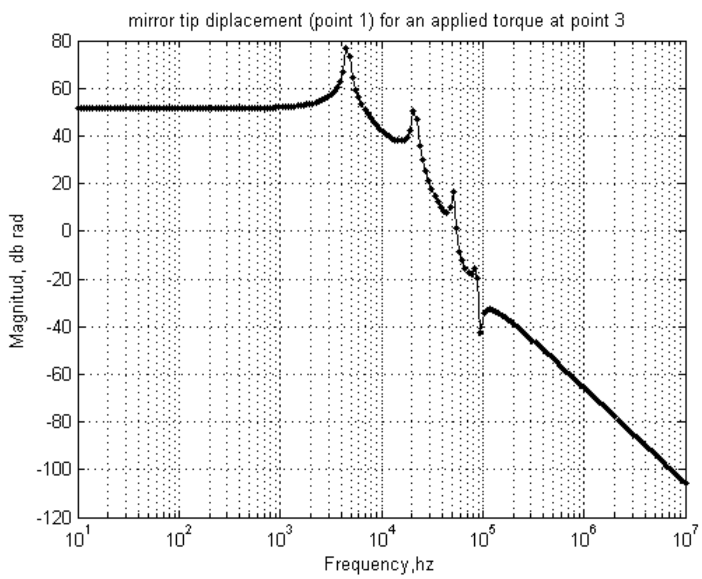

(b)

Figure- 3.3 Example transfer functions for 2D microscanner a) Torque applied at point 2 and rotational displacement measured at point 3. b) Torque applied at point 3 and rotational displacement measured at point 1

Chapter 4

DESIGN ANALYSIS

4.1 Introduction

After developing the state-space model of the physical system using FEM results, the validated model can be used for further design analyses. The state space model can be used for many design studies for performance prediction and optimization purposes. In this study, we are going to utilize the validated FEM to predict the performance of the system under anticipated disturbance sources. Additionally, we will conduct sensitivity analyses using two different approaches. The first one investigates the sensitivity of design parameters under the effect of disturbance sources. The second one investigates the effect of the design parameters on the natural frequencies of the microsystem.

4.2 Disturbance Analysis

The scanning capability of micro scanners can be significantly impacted by the disturbances coming from the outside sources. Since these devices are electro-statically or electro-magnetically actuated, driving electronics jitter, control loop sensor errors and thermal changes in the environment are the examples of disturbances that may affect the performance of the mirror during the operation mode.

Once the state space model of the micro scanner is created, the next step is to predict the performance when the model is subjected to the anticipated disturbances. The performance of optical micro system is directly related to its ability to steer the light beam in the desired direction [9]. In this disturbance analysis, the performance is defined as the rotation of the mirror about the x and y-axis. Inputs are defined as torque disturbances acting on the points 2 and 3 (see Figure- 3.1) and outputs are the amount of variance of the rotation at points 1 and 3. The variance of the rotation angle should be kept as small as possible in order to improve the performance of the mirror.

For stochastic linear systems driven by white noise, the solution of the Lyapunov equation represents the variance of the state vector [38]. The disturbance torque is modeled as the output of a first order shaping filter which is driven by unit intensity white noise.

When assessing the impact of disturbances on high-performance systems, it is critical that the disturbance models should be representative of the real operating conditions. An accurate plant model can still produce incorrect results when improperly modeled disturbances are applied to it. If design trades and decisions are based on the results of disturbance analysis that use mismodeled disturbances, the performance of the actual system in operation might be quite different from that which was predicted. As a result, the disturbance characterization process should be given as high a priority as the modeling process. This is especially true for high performance systems such as MEMS devices in which even low disturbance levels can cause the response to exceed requirements. [9]

Disturbances can be quantified by their frequency content, magnitude level, and the location and direction at which they enter the structure. The frequency content determines which modes of the structure can be excited and what the bandwidth of a control system should be. The magnitude level determines how much energy enters the structure. The location and direction information determine to what extent the modes in the frequency range can be excited. [39].

In this work, disturbances are modeled as outputs of a shaping filter which is driven by white noise in order to use for Lyapunov analysis [38]. The disturbance filter can be modeled in state-space form as:

$$\begin{aligned}\dot{\mathbf{x}}_{\mathbf{d}}(t) &= \mathbf{A}_{\mathbf{d}}\mathbf{x}_{\mathbf{d}}(t) + \mathbf{B}_{\mathbf{d}}u(t)\\ \mathbf{y}(t) &= \mathbf{C}_{\mathbf{d}}\mathbf{x}_{\mathbf{d}}(t)\end{aligned} \tag{4.1}$$

Where $\mathbf{A}_{\mathbf{d}}$, $\mathbf{B}_{\mathbf{d}}$ and $\mathbf{C}_{\mathbf{d}}$ are the state space matrices for the disturbance filter.

While generating the state space model of the mirror, mode shapes up to 100 KHz has been used. Consequently, a low pass disturbance filter that has a 100 KHz corner frequency which attenuates the disturbances that have frequencies higher than 100 KHz (equal to 627000 rad /sec) was designed. Frequency response and phase diagrams for the disturbance filter can be seen on Figure-4.1.

The magnitude content of the disturbance shaping filter is defined with a constant 'Disturbance Torque Intensity'. Torque intensity is used to scale the unit intensity white noise into the desired magnitude of the disturbance torques. The magnitude level of the disturbances is obtained from a previous work [9] that is handled for the Bimag scanner. The torque intensity level that is found for that specific kind of scanner is:

Torque intensity level = 1.75e-12 Nm. (4.2)

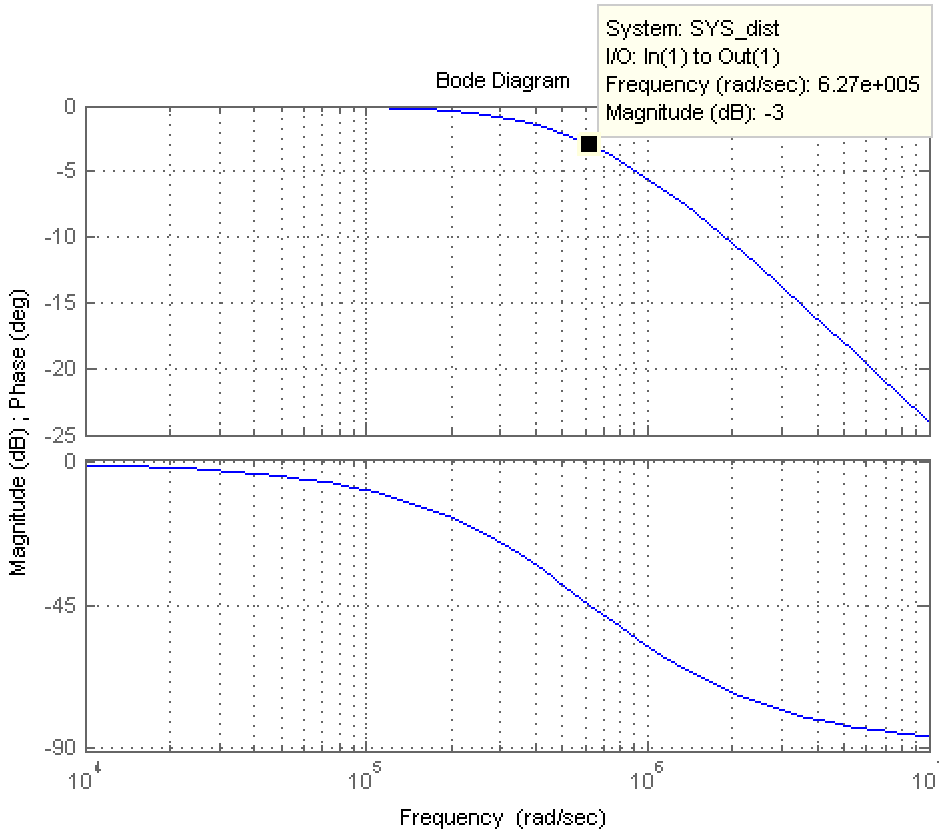

Figure-4.1 The frequency response and phase diagrams for the disturbance filter. The magnitude falls down quickly after the corner frequency.

Placing the state-space form of the disturbance filter in series with the plant equations from Equation (3.12) an overall system of the form can be represented as [9] (see Figure-4.2);

$$\begin{aligned}\dot{\mathbf{x}}(t) &= \mathbf{A}_{zd}\mathbf{x}(t) + \mathbf{B}_{zd}d(t) \\ \mathbf{y}(t) &= \mathbf{C}_{zd}\mathbf{x}(t)\end{aligned} \tag{4.3}$$

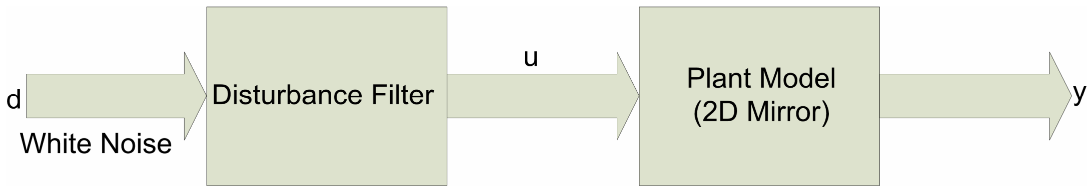

Figure-4.2 Disturbance shaping filter in series with plant model

Solution of the following steady-state Lyapunov equation leads to the state covariance matrix Σ_q.

$$\mathbf{A}_{zd}.\Sigma_{\mathbf{q}} + \Sigma_{\mathbf{q}}.\mathbf{A}_{zd}^{T} + \mathbf{B}_{zd}.\mathbf{B}_{zd}^{T} = 0 \tag{4.4}$$

This is a matrix equation with the unknown matrix Σ_q, and it can be solved using MATLAB [25].

The performance covariance matrix is given by [9]:

$$\Sigma_z = \mathbf{C}_{zd}\,\Sigma_q\,\mathbf{C}_{zd}^{T} \tag{4.5}$$

$$\Sigma_z = \begin{bmatrix} \sigma_{z1}^{2} & \sigma_{z1}\sigma_{z2} & \cdots & \sigma_{z1}\sigma_{zn} \\ \sigma_{z2}\sigma_{z1} & \sigma_{z2}^{2} & \cdots & \sigma_{z2}\sigma_{zn} \\ \vdots & \vdots & \ddots & \vdots \\ \sigma_{zn}\sigma_{z1} & \sigma_{zn}\sigma_{z2} & & \sigma_{zn}^{2} \end{bmatrix} \tag{4.6}$$

Where n is the total number of elements in one row or column. The diagonal terms of Σ_z represent the mean-square values of performance metrics and the root-mean-square (RMS) of these performance metrics can be obtained from the square roots of the diagonal entries. [9].

Using the Lyapunov approach, RMS estimates (in the sense of statistical steady state) can be calculated easily and directly by solving a single matrix Equation (4.4). It provides the exact mean-square values of the performance variables with subject to the accuracy of the disturbance and plant models. The diagonal terms of Σ_z represent the mean-square values $\sigma_{zi}^{\ 2}$ and the root-mean-square (RMS) values are simply σ_{zi} [9].

The 2D micro mirror is 1.5 mm in diameter and it has a resulting $\theta_{opt}.D$ product of 79.5 deg.mm for fast scan axis [12]. Where θ_{opt} is peak to peak optical scan angle and D is the diameter of the scanning mirror. Consequently, it satisfies the requirements for writing a SVGA (800x600) display according to the analysis given by Wine et al. [40]. The tilting angle of the micro mirror is defined as the mechanical scan angle. According to the study by Wine et al. [40], the mechanical scan angle of 6^o is needed for SVGA displays.

If this system is used to write a SVGA (800x600) display then 800 pixels will be written with the 6^o scan angle on a single line. Therefore the amount of radians corresponding to a pixel can be calculated using the following equation:

$$\frac{6^o.2\pi}{360^o} = 0.105 \ \textbf{rad} \qquad\qquad \frac{0.105}{800} = 1.31\text{x}10^{-4}\,\textbf{rad} \tag{4.7}$$

The image quality is not acceptable if the pixels are distorted by an amount of 20% [41].

$$1.31\text{x}10^{-4}\,\textbf{rad}.20/100 = \ 2.6\text{x}10^{-5}\,\textbf{rad} \tag{4.8}$$

Hence, variations of the scanner angular motion should be smaller than the value that is found at equation (4.8). Only then, the written image quality is in acceptable range. RMS value of the angular disturbances for the fast scan is $2.2\text{x}10^{-6}$ **rad** as it is shown at Table-4.1; as a result disturbances do not affect the scanner motion considerably.

Table-4.1 RMS values for torque disturbances

RMS value of the mirror angular displacement by Lyapunov approach	Fast scan direction Input point 3 vs. Output point 1	Slow Scan Direction Input point 2 vs. Output point 3
	$2.2\text{x}10^{-6}$ **rad**	$1.8\text{x}10^{-5}$ **rad**

4.3 Disturbance Sensitivity Analyses

Determining sensitivity of design parameters can provide useful information when the system does not meet the specified requirements. For systems with many design parameters, sensitivity information can identify which parameters in the system are the most significant. These parameters might be the focus of redesign efforts that attempt to improve the performance. In a previous work by Shi, Ramesh and Mukherjee [5] sensitivity analysis was carried out using the direct differentiation approach to compute the design sensitivity coefficients. The coupled electromechanical design sensitivities were presented by Allen, Raulli, Maute and Frangopol [6] for a reliability based analysis. Additionally Sigmund [7] presented the use of sensitivity analysis for topological optimization of electromechanical systems. Moreover, modal sensitivity analyses conducted for atomic force microscope probes by Chen and Huang [42] for investigating the effect of contact stiffness change on natural frequencies of the devices.

In order to compute the disturbance sensitivities following expression must be evaluated;

$$\frac{\partial \sigma_{zi}}{\partial p} = Sens.\ of\ a\ performance\ RMS\ w.r.t\ parameter\ p \qquad (4.9)$$

The finite difference technique was used to calculate the design parameter sensitivities. The design parameters were perturbed one at a time in the validated finite element analysis, the state space model was reconstructed for the perturbed system, and the performance was calculated using the Lyapunov approach. The performance difference between the perturbed system and the original system was then divided by the perturbed parameter step size and the sensitivity value was approximated. In order to compare sensitivities taken with respect to parameters of different units or magnitudes, the normalized sensitivities were computed as follows:

$$\frac{\dfrac{\sigma_{zi}\,perturbed - \sigma_{zi}\,original}{\sigma_{zi}\,original}}{\Delta p} = \frac{\partial \sigma_{zi}}{\partial p} \qquad (4.10)$$

The sensitivity analysis was performed for the 2D scanner for the following design parameters; thickness of slow scan flexure (Tss), width of slow scan flexure (Wss), length of slow scan flexure (Lss), first diameter of the mirror (L1), second diameter of the mirror (L2) and the density of the overall structure (see Figure-3.1).

Table 4.2 tabulates the physical parameter sensitivities for the torsional MEMS scanner. Among the computed sensitivities, the greatest sensitivity belongs to the slow scan flexure beam length and thickness. For the case, when we apply an input torque at point 3, 1% increase in the flexure length and thickness will result a 2.16% increase and 1.93% decrease in the RMS performance value of point 1, respectively. A similar behavior is observed when the input torque is applied at point 2 and the output RMS value is measured at point 3 although the percentages vary slightly compared to the previous case. Since the performance is defined as the deviation of the specified point under random disturbances, increasing the beam thickness results in an increase in system stiffness and a decrease in this deviation. When the length of the flexure beam is increased, an adverse effect is expected. Increasing the width of the slow scan flexure results a better performance for both performance output locations. The mirror dimensions are directly related to optical resolution of the system so they are not generally included in the structural redesign efforts. However, the sensitivity results show that they are as significant as the flexure dimensions in terms of determining the performance of the 2D scanner.

Table 4.2- Disturbance Sensitivity Analysis

	Input 3 vs. output 1 (%)	Input 2 vs. output 3 (%)
Slow Scan Flexure Width (Wss)	-0.59	-0.60
Slow Scan Flexure Length (Lss)	2.16	1.07
Slow Scan Flexure Thickness (Tss)	-1.93	-1.97
Density of the Structure	-0.25	-0.25
1^{st} Diameter of mirror (L1)	-0.61	-0.25
2^{nd} Diameter of mirror (L2)	0.03	-0.33

4.4 Modal Sensitivity Analysis

Micro scanner mirrors are operated dynamically at a specific natural frequency, which is usually a torsional mode of its operation, for generating high movement by low input power. In order to improve the performance of the micro scanners, this specific frequency can be increased by physical parameter modifications and optimization methods for improving the image resolution [13]. The change of a physical parameter causes the stiffness and inertia change and effectively a shift in modal frequencies. Hence, the designer can modify and optimize the modal frequencies of a micro structure with a wise selection of physical parameters.

In this manner, modal sensitivity analysis, which is defined as the change of the specific mode frequency according to a physical parameter perturbation, can be used for identifying which parameters of the system cause the most significant effect on the modal frequencies. And this information can be used to improve the performance of the system.

As in the case of disturbance sensitivity analysis, the finite difference technique was used to calculate the modal parameter sensitivities. The design parameters were perturbed one at a time in the finite element analysis and the modal analysis was performed in ANSYS. The frequency change between the perturbed system and the original system was then divided by the perturbed parameter step size and the sensitivity value was approximated. In order to compare sensitivities taken with respect to parameters of different units, the normalized sensitivities were computed as follows:

$$\frac{\dfrac{f_{new,i} - f_{orig,i}}{f_{orig,i}}}{\Delta p} = \text{Modal Sensitivity for the specific mode} \qquad (4.11)$$

Where $f_{new,i}$ stands for the new model's i^{th} mode shape's frequency and $f_{org,i}$ stands for the original model's i^{th} mode shape's frequency. In order to normalize the effect of each parameter change, Δp term which is the parameter step size change is used in the sensitivity calculation.

The physical parameters that are used to construct the modal analysis sensitivity calculations are; first diameter of the mirror (L1), second diameter of the mirror (L2), length of fast scan flexure (Lfs) , length of slow scan flexure (Lss), the density of the overall structure (Ro), thickness of the mirror (Tm), thickness of slow scan flexure (Tss) , width of slow scan flexure (Wfs) and width of slow scan flexure (Wss). These design parameters are shown in Figure-3.1.

Table 4.3 shows modal parameter sensitivity values for each parameter change. While constructing the table each parameter was changed by 1% and the modal sensitivities were calculated through the use of the Equation (4.11). The mode descriptions for each mode can be seen on Table 2.1.

Table-4.3 Table for modal sensitivity calculations for different physical parameters.

(All values are in %)

	L1	L2	Lfs	Lss	Ro	Tm	Tss	Wfs	Wss
Torsional Mode	0.033	-0.15	-0.18	-0.7	-0.5	-0.09	1.34	0	0.4
Out-of-plane translation	-0.17	-0.13	-0.075	-1.72	-0.5	-0.24	1.42	-0.014	0.42
Out-of-plane rocking (in-phase)	-0.049	-0.11	-0.09	-1.52	-0.5	-0.25	1.42	-0.015	0.42
Out-of-plane rocking (out-of-phase)	-0.71	-0.19	-0.27	-0.014	-0.5	-0.33	0.03	1.01	0.08
Out-of-plane translation (out-of-phase)	-0.21	-0.08	-0.7	0.055	-0.5	0.17	-0.03	0.17	0.004

As it can be observed from Table 4.3, the first mode (torsional mode) is most sensitive to the variation of the physical parameter “Tss” which is the thickness of slow scan flexure. If the thickness of the slow scan flexure is changed by an amount of 1%, the torsional frequency will increase with an amount of 1.34%. This means that the torsional mode is most sensitive to the thickness of the slow scan flexure. In the same manner, the out-of-plane translation mode is most sensitive to the length of the slow scan flexure, “Lss”. The most sensitive physical parameters for the other modes can be seen in Table 4.3. For out-of- plane (in-phase) mode, the most sensitive parameter is “Lss”, for out-of-plane rocking (out-of-phase) mode it is “Wfs” and for out-of-plane translation (out-of-phase) mode it is “Lfs”. According to this modal sensitivity data, the frequency modifications can be made effectively in the design process or the data can be used for optimization purposes for further design studies.

Chapter 5

DISCUSSION AND CONCLUSION

A generalized design approach and a model validation methodology were developed in order to predict and also improve the performance of micro systems. The first step in our design approach was to build the experimental modal analysis setup to verify the finite element models of the micro systems. The experimental setup included special equipment such as a LDV, a CCD camera, microscope system and a data acquisition system with interface programs to acquire, collect and process the vibration data. We measured the out-of-plane vibrations of the micro scanner mirror to demonstrate the developed methodologies. After the vibration data was collected, it was transferred to a modal analysis software, MeScope. The mode shapes, modal frequencies and damping coefficients were extracted using the transfer functions obtained at various points on the structure.

In parallel to the experimental studies, the finite element model of the micro mirror was built in order to perform various design studies. The FEM was validated using the experimental measured data. The mode shapes and modal frequencies of the model predictions and experiment results were compared to identify the inaccuracies in the modeling assumptions. The FEM was updated and corrected such that we had a better match between the experiments and numerical results. After we were satisfied with the FEM predictions, the next step was to predict the performance of the system under the anticipated disturbance sources. The state space representation of the system was used for disturbance analysis which was performed using Lyapunov approach to obtain root-mean square (RMS) values of the mirror rotation angle under the effect of a disturbance torque. The disturbance analysis was combined with the sensitivity analysis to determine the most critical design parameters that effect the performance of the system. The slow scan flexure dimensions were found to be the most significant parameters when the disturbances were effective on the system. Modal sensitivity analysis of the system was also performed to identify the most critical design parameters in order to change the modal frequencies. The modal sensitivity analysis showed that each mode of the system was sensitive to a different design parameter. However, fast scan and slow scan flexure dimensions were the most significant ones among the other parameters.

Sensitivity analysis has proven itself to be an extremely valuable tool especially when the MEMS have many design parameters. The modal sensitivity analsis provides valuable information especially when the high frequency and/or separation of critical vibration modes are the design requirements of the micro device. Knowing which parameter is the most critical one, the designer can alter the modal frequencies very efficiently and easily.

Another study that was performed in this thesis was using the analytical formulations to predict the modal frequencies of the system. Although the formulations were very successful in calculating the first couple of modes, the higher frequency behavior was not predictable with these formulations. However, at the initial design stage these formulations are still valuable when the designer needs quick results especially when the finite element model of the system is not available.

Although we have included the details of the experimental setup and the testing methods for the in-plane vibration measurements, this work is still in progress. Adding the in-plane measurement capability to the current setup will enable a complete 3D dynamic characterization of the micro devices. Another future study that may follow this study could be the optimization of the design parameters to improve the performance of the micro devices. Most of the optimization algorithms require the sensitivity information which was obtained with the sensitivity analysis performed in this thesis.

BIBLIOGRAPHY

[1] H. Li, E. K. Antonsson, "Evolutionary Techniques in MEMS Synthesis," ASME Desing Engineering Technical Conferences, September 1998

[2] N. Zhou, A. Agogino, K. S. J. Pister, "Automated design synthesis for Micro-Electro-Mechanical Systems (MEMS)," Proceedings of DETC 2002: Design Automation, Montreal, Canada, September 2002

[3] T. Mukherjee, G. K. Fedder, "Structured design of microelectromechanical systems," Proceedings of the 34th annual conference on Design Automation, Anaheim, CA, US, 1997, pp. 680-685

[4] Y. Zang, R. Kamalian, A. M. Agogino, C.H. Sequin, "Hierarchical MEMS Synthesis and Optimization," Smart Structures and Materials 2005: Smart Electronics, MEMS, BioMEMS and Nanotechnology, Proceedings of SPIE Vol. 5763, pp. 96-106

[5] F. Shi, P. Ramesh and S. Mukherjee "Simulation methods for micro-electro-mechanical structures (MEMS) with application to a microtweezer" Comput. Struct. *(*USA*).* Vol. 56, no. 5, pp. 769-783. 3 Sept. 1995

[6] M. Allen, M. Raulli, K. Maute, D. M. Frangopol "Reliability-based analysis and design optimization of electrostatically actuated MEMS" Comput. Struct. Vol. 82, no. 13-14, pp. 1007-1020. May 2004

[7] O. Sigmund, "Design of multiphysics actuators using topology optimization – Part I: One material structures" Computer Methods in Applied Mechanics and Engineering, Vol. 190, Number 49, 2001, pp. 657-6604(28)

[8] C. Ataman, "Design, Modeling and Characterization of Electrostatically Actuated Microscanners," M. S. Thesis, Koc University, September 2004

[9] C. Meral, “Sensitivity Analysis and Performance Prediction Methodology for MEMS Design,” M. S. thesis, Koc University Mechanical Engineering, August 2005.

[10] H. Urey, “Retinal Scanning Displays”, Encyc. of Optical Engineering, Marcel-Dekker, 2003.

[11] A. Wolter, H. Schenk, E. Gaumont, H. Lakner, “MEMS microscanning mirror for barcode reading: from development to production,” SPIE Proc. of MOEMS Display and Imaging Systems II, vol. 5348, pp. 32-39, 2004.

[12] A. D. Yalcinkaya, H. Urey, T. Montague, D. Brown, and R. Sprague, “Two-axis Electromagnetic Microscanner for High Resolution Displays, ” IEEE/ASME Journal of Microelectromechanical Systems, vol. 15 (4), pp.786-794, 2006

[13] H. Urey, “High performance resonant MEMS scanners for display and imaging applications,” Optomechatronic micro/nano components, devices, and systems conference, Proc.SPIE, Vol.5064, Philadelphia, Pennsilyvania, October 2004.

[14] O. B. Ozdoganlar, B. D. Hansche, T. G. Carne, “Experimental modal analysis for Microsystems,” presented at IMAC’21, Kissimmee, FL, and in Proc. of 21st International Modal Analysis Conference (IMAC), 2003.

[15] C. Rembe, R. Kant, R. S. Muller, “Optical Measurement Methods to Study Dynamic Behavior in MEMS,” Proc. SPIE 2001, vol.4400, pp. 127-37

[16] W.Hemmert, M.S.Mermelstein, D.M.Freeman, “Nanometer resolution of three dimensional motions using video interference microscopy,” Proc.IEEE MEMS’99 (Orlando, Florida) pp. 302-308

[17] S.Petitgrand, A.Bosseboeuf, “Simultaneous mapping of out-of-plane and in-plane vibrations of MEMS with (sub) nanometerresolution, ” J.Micromech.Microeng., vol. 14 (2004) pp. 97-101.

[18] S. Petitgrand, R. Yahiaoui, K. Danaie, A. Bosseboeuf, J.P. Gilles, “3D measurement of micromechanical devices vibration mode shapes with a stroboscopic interferometric microscope,” Optics and Lasers Eng., vol. 36(2001) pg 77-101.

[19] James S. Burdess, Alun J. Harris, David Wood, Robert J. Pitcher, and David Glennie, “A System for the Dynamic Characterization of Microstructures,” Journal of Microelectromechanical Systems; (1997); Vol. 6 (4) ; pp. 322-328.

[20] Y.F.Chou, L.C.Wang, “On the Modal Testing of Microstructures: Its Theoretical Approach and Experimental Setup, ” Journal of Vibrations and Acoustics, vol. 123, pp.104-109.

[21] M. M. Guillemot-Amadei, L. Petit, L. Lebrun, R. Briot, P. Gonnard, “A non-contact measurement technique for piezoelectric transducers,” Meas.Sci.Technol., vol 6 (1995), pp. 458-466.

[22] Polytec OFV-551/552 Fiber-Optic Interferometer Datasheet

[23] Polytec manual microscope scan unit, MSV-50, User Manual

[24] http://www.ni.com/labview/

[25] http://www.mathworks.com/

[26] ME’scope VES operating manual, Version 3.0, September 2001

[27] Y. H. Cho, A. P. Pisano, and R. T. Howe, “Viscous damping model for laterally oscillating microstructures,” J.Microelectromech.Syst., vol. 3, no. 2, pp. 81–87, 1994.

[28] N.Uchida, K.Uchimaru, M. Yonezawa, M. Sekimura, “Damping of micro electrostatic torsion mirror caused by air-filmviscosity,” Proc.IEEE MEMS 2000 (Miyazaki, Japan) pp. 449-454

[29] B.Serio, J. J. Hunsinger, B. Cretin,“In-plane measurements of microelectromechanical systems vibrations with nanometer resolution using the correlation of synchronous images,” Review of Scientific Instruments, vol. 75 (10), pp. 3335-3341, (2004)

[30] Polytec Laser Measurement Systems, LM INFO Special Issue 1/2005

[31] http://www.lumileds.com/

[32] ANSYS Release 8.1 Documentation

[33] Shabana, Theory of Vibration, vol. 2, Springer-Verlag, 1991

[34] H. Urey, C..Kan, W. O. Davis, “Vibration mode frequency formulae for micromechanical scanners,” J. Micromech. Microeng. Vol. 15 (2005), pp. 1713-1721

[35] R. D. Blevins , “Formulas for natural frequency and mode shape,” Reprint edition, Krieger Publishing Company, Florida, 1984 , page 48

[36] R. C. Dorf, R. H. Bishop, “Modern Control Systems,” International edition, Pearson Education Inc., US, c2005

[37] M. R. Hatch, B. Raton, “Vibration Simulation Using MATLAB and ANSYS” Chapman & Hall CRC c2001.

[38] Z. Gaji´c, M. T. J. Qureshi , “Lyapunov Matrix Equation in System Stability and Control”. San Diego : Academic Press, c1995.

[39] H. L. Gutierrez and D. W. Miller “Performance Assessment and Enhancement of Precision Controlled Structures During Conceptual Design”, February 1999

[40] D. W. Wine, M. P. Helsel, L. Jenkins, H. Urey, T. D. Osborn, “Performance of a Biaxial MEMS-Based Scanner for Microdisplay Applications,” Conference on MOEMS and Miniaturized Systems, SPIE Vol. 4178, pp. 186-196, CA, US, (2000)

[41]H. Urey, D. Wine, T. Osborn, "Optical performance requirements for MEMS-scanner based microdisplays," Conference on MOEMS and Miniaturized Systems, SPIE Vol. 4178, pp. 176-185, CA, US, (2000)

[42] K. N. Chen, J. C. Huang, “Analysis of tip effects on the dynamic characteristics of V-shaped atomic force microscope probes,” Proceedings of the 2005 International Conference on MEMS, NANO and Smart Systems (ICMENS’05), pp. 65-68

PUBLICATIONS

O. Anac, I. Basdogan, “Application of a Design Methodology Using a 2D Micro Scanner,” Technical Proceedings of the 2006 NSTI Nanotechnology Conference and Trade Show, vol. 3, pp. 594-597, Boston (MA), US, May 2006

O. Anac, I Basdogan, “Model Validation Methodology for Design of Micro Systems, ” Proceedings of ESDA2006, 8th Biennial ASME Conference on Engineering Systems Design and Analysis, Torino, Italy, July 2006

O. Anac, I. Basdogan,” Model Validation and Performance Prediction in the Design of Micro Systems,” to be submitted to Journal of Micromechanics and Microengineering.

VITA

Ozan Anaç was born in Burdur, Turkey, in 1981. He received his B.Sc. degree from Mechanical Engineering Department of Middle East Technical University, Ankara, in 2004. Same year, he joined Department of Mechanical Engineering at Koç University, Istanbul, as an M.Sc candidate. He is a student member of ASME. Ozan Anaç is planning to pursue a Ph.D degree at University of California-Irvine.